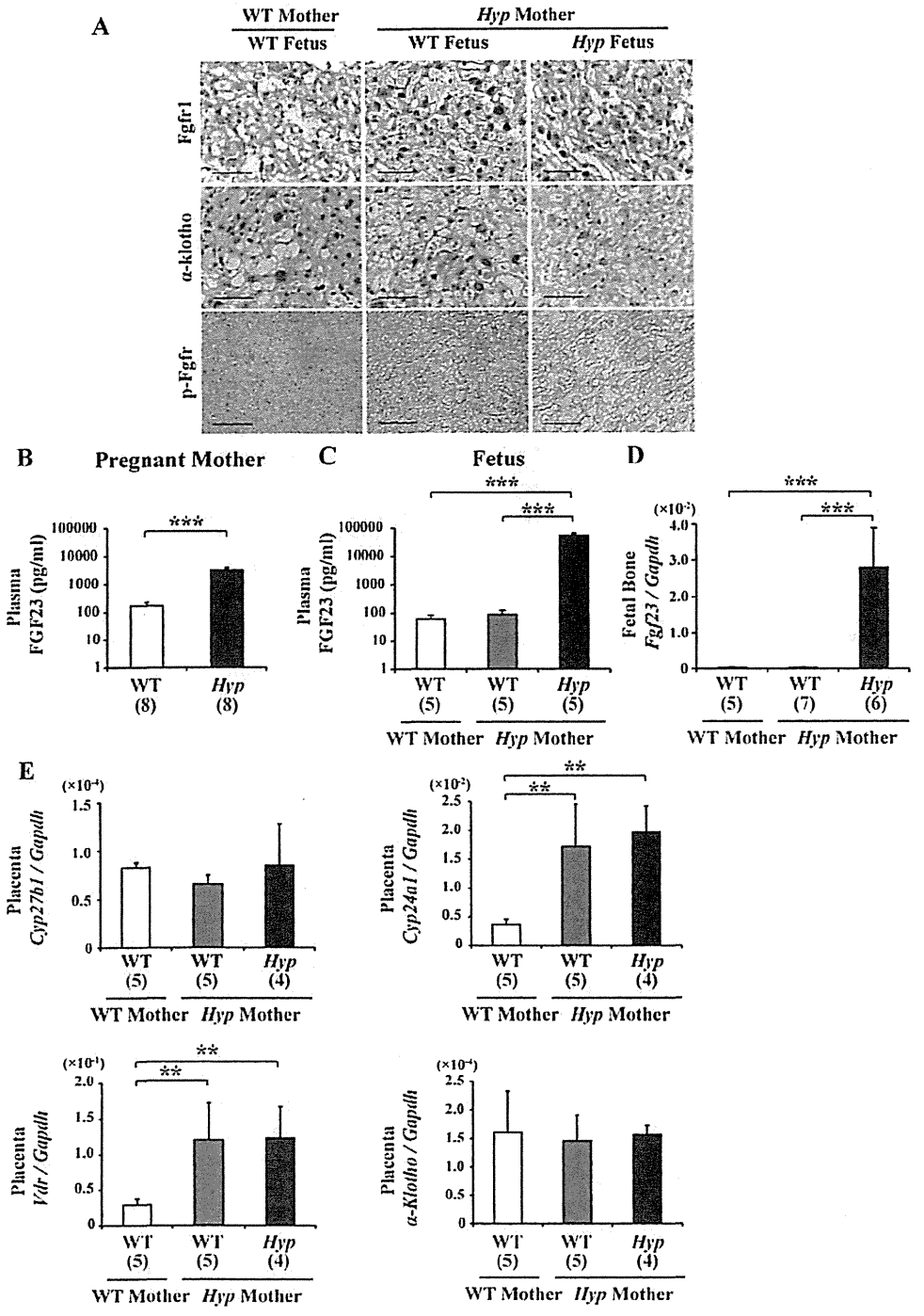

Fig. 3. Increased expression of *Cyp24a1* in the placentas of fetuses from *Hyp* mothers. (*A*) Immunohistochemical staining of the placentas of male fetuses from *Hyp* mothers and WT mothers at E18.5 using antibodies against the Fgfr1, α-Klotho, and phosphorylated Fgfr (p-Fgfr). There was no obvious difference in staining Fgfr1 and α-Klotho among the genotypes, whereas the signals of p-Fgfr were stronger in the placentas of fetuses from *Hyp* mothers, regardless of the fetal genotypes. Sections were counterstained with hematoxylin. Scale bars = 50 μm. (*B*, *C*) Plasma levels of intact FGF23 in *Hyp* and WT mothers (*B*) and their fetuses (*C*) at E18.5. Heterozygous *Hyp* females or WT females were mated with WT males, and plasma samples were obtained from them and their male fetuses at E18.5. Fetal plasma from genetically identical littermates of one mother was pooled and assayed as one sample. The level was 20-fold higher in *Hyp* fetuses than in *Hyp* mothers. (*D*) Expression of *Fgf23* in the fetal bones. Fetal bones were harvested from *Hyp* and WT male fetuses of *Hyp* mothers and from WT male fetuses of WT mothers at E18.5 and were used for real-time PCR to examine the expression of *Fgf23*. The expression of *Fgf23* was increased in the bones from *Hyp* fetuses. (*E*) Placental gene expression. Placentas were harvested from *Hyp* and WT male fetuses of *Hyp* mothers and from WT male fetuses of WT mothers at E18.5 and were used for real-time PCR to examine the expression of the indicated genes. The expression of *Cyp24a1* and *Vdr* was increased in the placentas of fetuses from *Hyp* mothers. The sample numbers are indicated in parentheses. Data are shown as the mean ± SD. $^{*}p < 0.05$; $^{**}p < 0.01$; $^{***}p < 0.001$.

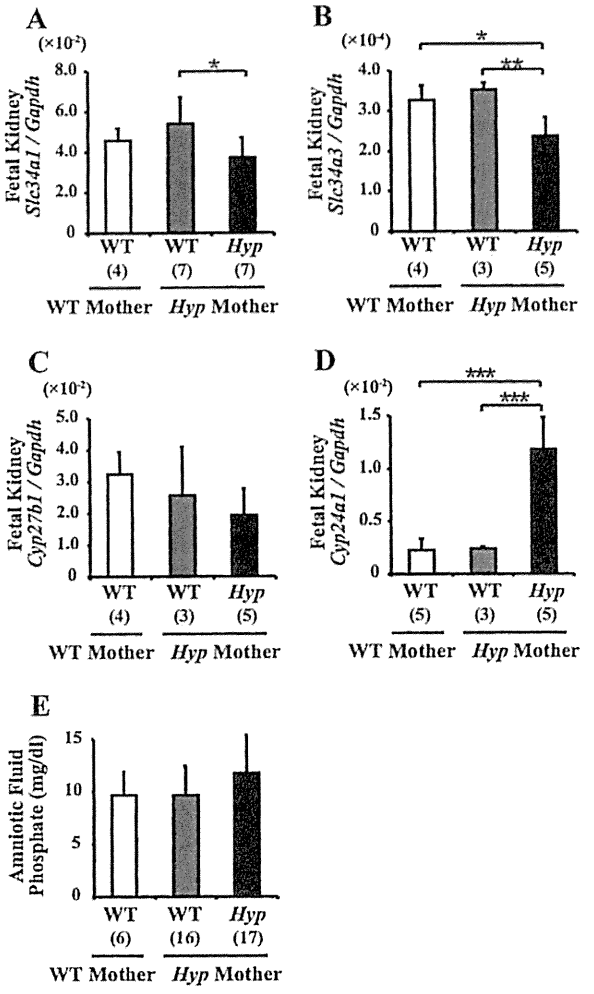

Fig. 4. Altered gene expression in fetal kidney of *Hyp* mice. (*A–D*) Kidneys were harvested from *Hyp* and WT male fetuses of *Hyp* mothers and from WT male fetuses of WT mothers at E18.5 and were used for real-time PCR to examine the expression of *Slc34a1* (*A*), *Slc34a3* (*B*), *Cyp27b1* (*C*), and *Cyp24a1* (*D*). The copy number of the target cDNA in each sample was estimated by referring to a standard curve and was normalized based on that of *Gapdh*. In the kidneys of *Hyp* fetuses, the expression of *Slc34a1* and *Slc34a3* was decreased and that of *Cyp24a1* was increased. (*E*) Concentration of Pi in the amniotic fluid. The sample numbers are indicated in parentheses. Data are shown as the mean ± SD. $^{*}p < 0.05$; $^{**}p < 0.01$; $^{***}p < 0.001$.

mothers (Fig. 7*G*). The fetal levels of 1, 25(OH)$_2$D were measured as pooled samples collected from 20 fetuses in each group because 350 μL of plasma was required for the measurement. Although we could not perform statistical analysis, the levels of 1,25(OH)$_2$D in the fetuses of *Hyp* mothers tended to be decreased more than that in the fetuses of WT mothers (Fig. 7*H*). The lower levels of 25OHD and the increased 24,25(OH)$_2$D/25OHD ratio suggested that the increased placental expression of *Cyp24a1* had an impact on vitamin D metabolism in the fetuses of *Hyp* mothers. We cannot exclude the possibility that the high fetal FGF23 in *Hyp* fetuses also might have some roles in the regulation of fetal 1,25(OH)$_2$D levels by altering the expression of *Cyp24a1* in fetal kidney because the 1,25(OH)$_2$D level in *Hyp* fetuses was lower than that in their WT littermates (Fig. 7*H*).

Discussion

FGF23 is mainly produced by osteocytes in bone and exerts effects on distant organs, including the kidney, in an endocrine fashion. Unique among FGFs, FGF19 and -21 as well as FGF23 act in an endocrine fashion to regulate diverse physiological processes and have been classified as the FGF19 subfamily. Low binding affinity to heparin/heparan sulfate has been suggested to confer endocrine function on the members of the FGF19 subfamily, by allowing them to escape heparan sulfate surrounding the cells from which they are produced.[3,31] In their target organs, the members of the FGF19 subfamily require α-Klotho (FGF23) or β-Klotho (FGF19 and FGF21) to evoke their signals. FGF23 was shown to bind to the FGF receptor (FGFR) and α-Klotho to form a complex and induced the phosphorylation of the FGFR substrate 2α (FRS2α) and ERK1/2 downstream.[16,17] Therefore, α-Klotho-expressing organs have been considered to be targets of FGF23.

Based on our previous finding that human placenta expresses α-Klotho,[22] we hypothesized that the placenta also might be a target of the endocrine action of FGF23. In the current study, we used mouse models to test this hypothesis, although human and mouse placentas differ in their structure. In the mouse placenta, the labyrinth zone provides the feto-maternal interface where tortuous maternal and fetal vasculatures develop and maternal and fetal blood flows in a countercurrent manner to maximize the exchange of nutrients, ions, and gases. In the labyrinth zone, fetal-derived mononuclear trophoblasts and syncytiotrophoblasts face the maternal blood. In humans, numerous villi containing fetal vessels branch into the intervillous spaces filled with maternal blood. Syncytiotrophoblasts cover the face of the villi and exchange nutrients, ions, and gases between the fetal and maternal blood.[29,32] Despite the difference in structure, the expression patterns of the genes involved in FGF23 signaling were similar between normal mouse and human placentas (Fig. 1*A*, *B*). In addition, co-expression of FGFR1 and α-Klotho at the syncytiotrophoblasts, which provide feto-maternal interface, was observed in both mouse and human placentas (Fig. 1*C*, *D*, and Supplemental Fig. S2). These results suggest that common mechanisms are involved in FGF23 signaling between mice and humans.

Our results shown here demonstrate that in pathological conditions with elevated level of circulating FGF23, it exerts effects on the placenta and increases the expression of *Cyp24a1*, the gene encoding the critical enzyme in vitamin D metabolism. First, the placental expression of *Cyp24a1* was increased in the fetuses of *Hyp* mothers with high levels of FGF23 compared with the fetuses of WT mothers (Fig. 3*B*, *E*). Second, in ex vivo experiments using the organ culture of placentas from WT mice, treatment with *Hyp* plasma resulted in a marked increase in *Cyp24a1* expression, which was abolished by the simultaneous addition of the neutralizing antibody against FGF23 (Fig. 5*A*). In addition, treatment of the cultured placentas with recombinant FGF23 resulted in the increased *Cyp24a1* expression (Fig. 5*B*). These observations confirmed that high levels of FGF23 caused elevated placental expression of *Cyp24a1* in the fetuses of *Hyp* mothers. Finally, direct injection of a recombinant FGF23 into the placentas of WT mice induced the expression of *Cyp24a1* and *Egr-1* (Fig. 6*A*, *B*). These results together indicate that pathological

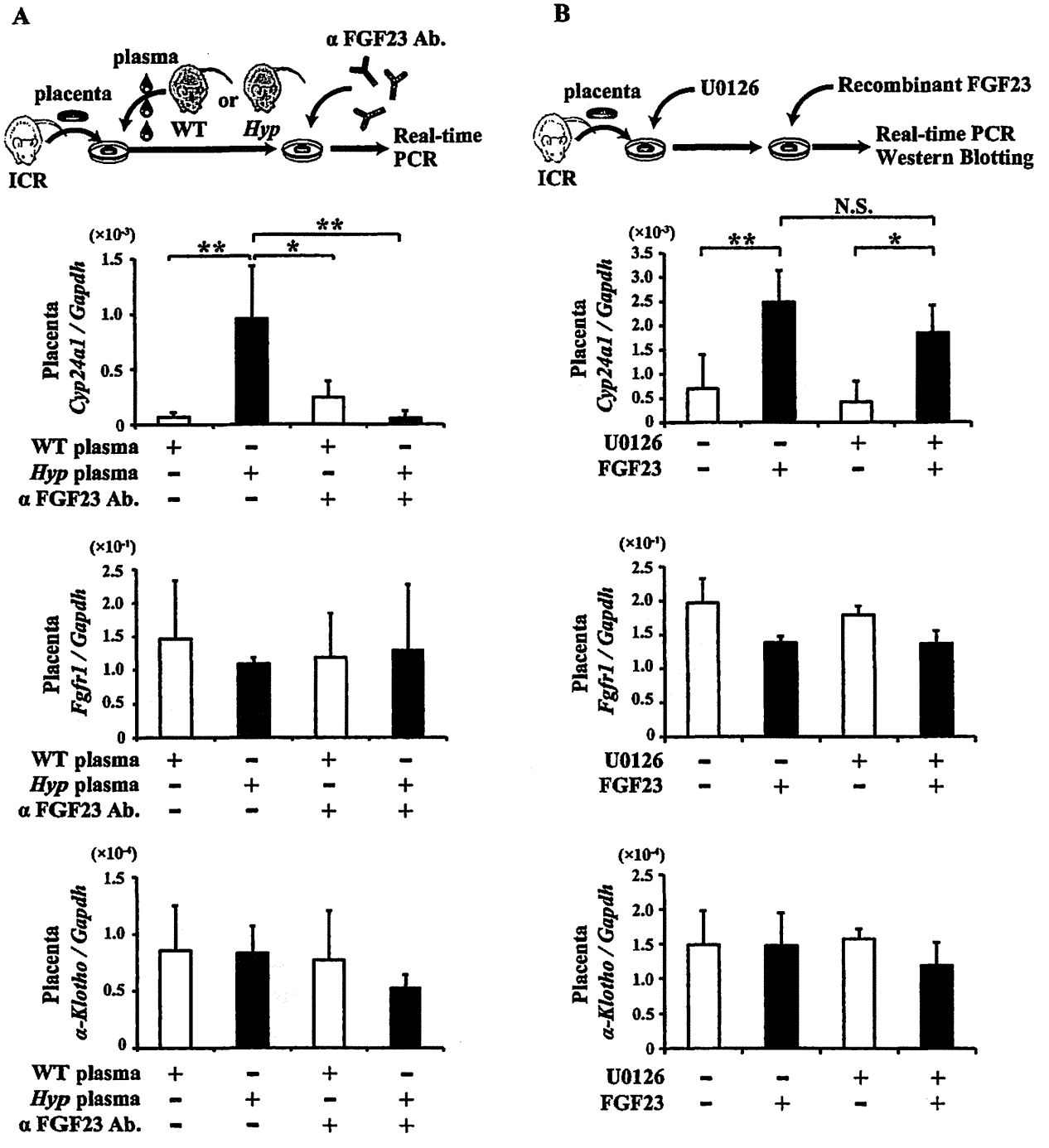

Fig. 5. Effects of *Hyp* plasma and anti-FGF23 antibody on *Cyp24a1* expression in WT placenta in culture. (*A*) The placentas of WT ICR mice (E18.5) were incubated with 10% of plasma from WT C57BL/6J or *Hyp* pregnant mothers in the presence or absence of the anti-FGF23 antibody (2 μg/mL). After 30 minutes' incubation at 37°C, the placentas were collected for real-time PCR analyses to examine the expression of *Cyp24a1*, *Fgfr1*, and *α-Klotho*. The expression of *Cyp24a1* was increased by treatment with *Hyp* plasma, which was abolished by the simultaneous addition of anti-FGF23 antibody. (*B*) The placentas of WT ICR mice (E18.5) were incubated with an MEK inhibitor (U0126: 10 μM) for 30 minutes at 37°C. Then, recombinant FGF23 (500 ng/mL) was added to the media, and the samples were incubated for an additional 15 and 120 minutes at 37°C to extract proteins and RNA, respectively. The RNA was used for real-time PCR analyses to examine the expression of *Cyp24a1*, *Fgfr1*, and *α-Klotho*. The protein was used for Western blotting to examine phosphorylation of ERK1/2. The expression of *Cyp24a1* was increased by treatment with recombinant FGF23, which was not cancelled by the cotreatment with U0126. Data are shown as the mean ± SD. $^{*}p < 0.05$; $^{**}p < 0.01$. N.S. = not significant. $n = 4$ to 5 placentas per group.

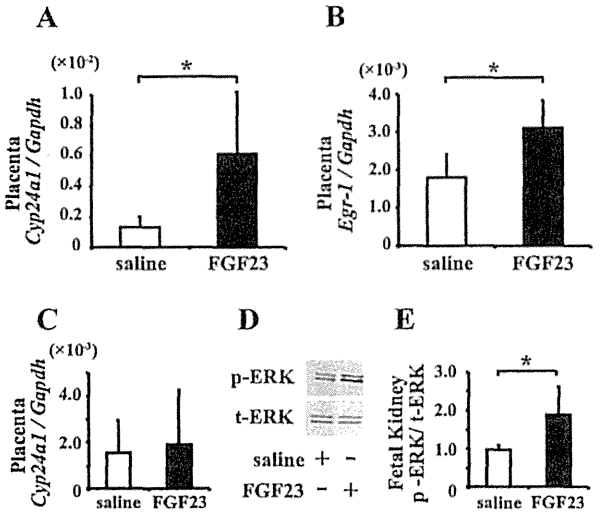

Fig. 6. Direct injection of recombinant FGF23 into the placenta or fetus. (*A*, *B*) Effects of the administration of recombinant FGF23 into the placenta on the expression of *Cyp24a1* (*A*) and *Egr-1* (*B*). E18.5 WT ICR pregnant mice were anesthetized and the uteri were exposed. Forty nanograms of recombinant FGF23 (R179Q) (black bars) or the equivalent volume of saline (white bars) was directly injected into the placentas. Thirty minutes later, the placentas were harvested and used for real-time PCR. The direct injection of recombinant FGF23 into the placenta induced the expression of *Cyp24a1* and *Egr-1* in placenta. $n = 5$ placentas per group. (*C–E*) Effects of the administration of recombinant FGF23 into the fetuses on the placental gene expression. E18.5 WT ICR pregnant mice were anesthetized and the uteri were exposed. Four hundred nanograms of recombinant FGF23 (R179Q) (black bars) or the equivalent volume of saline (white bars) was injected intraperitoneally into the fetuses. Thirty minutes later, the placentas and fetal kidneys were harvested and used for real-time PCR (*C*) and Western blotting (*D*, *E*), respectively. Although the injection of recombinant FGF23 into the fetuses increased the phosphorylation of ERK1/2 in the fetal kidneys (*D*, *E*), it did not alter the placental expression of *Cyp24a1* (*C*). $n = 7$ fetuses per group. Data are shown as the mean ± SD. $^*p < 0.05$.

levels of FGF23 directly act on the placenta to induce the expression of *Cyp24a1*. As for *Cyp27b1*, another target of FGF23 in the kidney, its placental expression was marginal, and we could not detect a difference among the genotypes (Fig. 3*E*). The placental expression of *Vdr* was also increased in the fetuses of *Hyp* mothers by a mechanism not yet understood. The maternal FGF23, not fetal FGF23, is likely to be responsible for the regulation of placental *Cyp24a1* expression because intraperitoneal injection of recombinant FGF23 into the fetuses failed to upregulate the placental *Cyp24a1* expression (Fig. 6*C*).

To clarify whether the increase in the placental expression of *Cyp24a1* had an impact on vitamin D metabolism of the fetuses of *Hyp* mothers, we measured the plasma levels of vitamin D metabolites. The 25OHD-24-hydroxylase converts 25OHD to $24,25(OH)_2D$ and $1,25(OH)_2D$ to $1,24,25(OH)_3D$. The plasma levels of 25OHD in the fetuses of *Hyp* mothers were lower than those in the fetuses of WT mothers, although the level of 25OHD in *Hyp* mothers was similar to that in WT mothers (Fig. 7*A*, *B*). In addition, the $24,25(OH)_2D$/25OHD ratio tended to be increased in the fetuses of *Hyp* mothers than in those of WT mothers (Fig. 7*E*). The

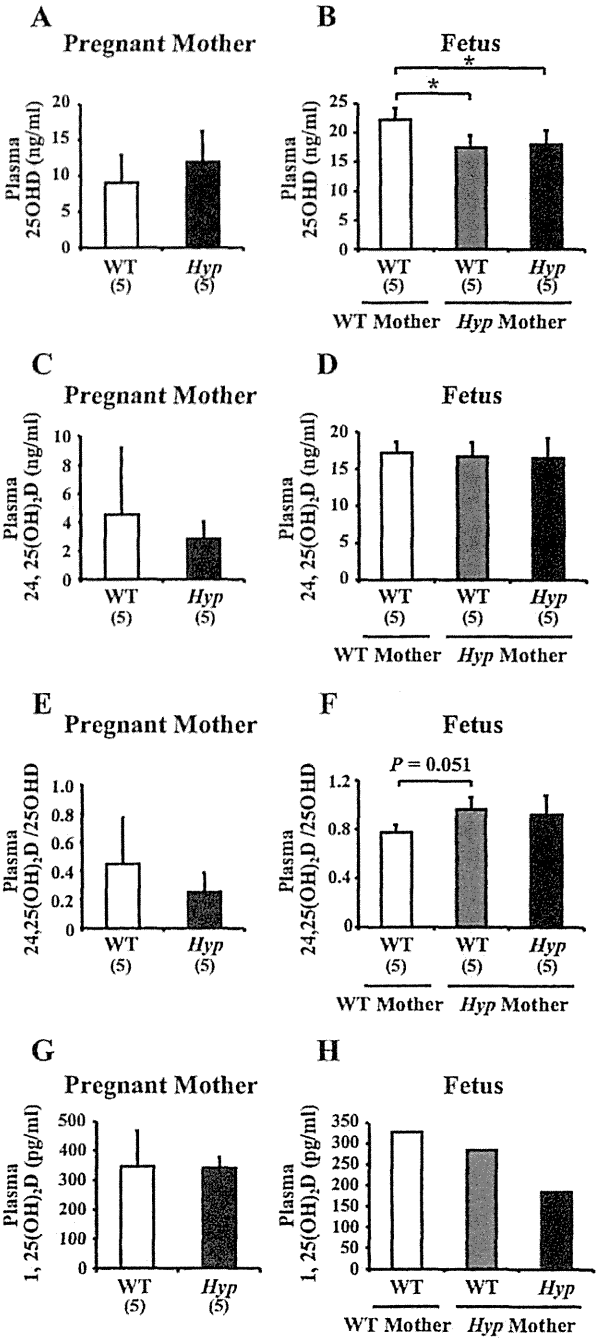

Fig. 7. Plasma levels of vitamin D metabolites in WT and *Hyp* pregnant mothers and their fetuses. Plasma levels of 25OHD in *Hyp* and WT pregnant mothers (*A*) and in their fetuses (*B*) at E18.5. The levels of 25OHD in the fetuses from *Hyp* mothers were lower than those from WT mothers. Plasma levels of $24,25(OH)_2D$ in pregnant mothers (*C*) and in their fetuses (*D*) at E18.5. The ratio of the concentration of $24,25(OH)_2D$ to that of 25OHD in pregnant mothers (*E*) and in their fetuses (*F*). Plasma levels of $1,25(OH)_2D$ in pregnant mothers (*G*) and in their fetuses (*H*) at E18.5. The sample numbers are indicated in parentheses. The fetal levels of $1,25(OH)_2D$ were measured as pooled samples collected from 20 fetuses in each group because 350 μL of plasma was required for the measurement. Data are shown as the mean ± SD. $^*p < 0.05$.

levels of $1,25(OH)_2D$ in the fetuses of *Hyp* mothers tended to be decreased than that in the fetuses of WT mothers (Fig. 7H). These results suggested that the high levels of FGF23 in *Hyp* mothers resulted in the accelerated conversion of 25OHD to $24,25(OH)_2D$ and $1,25(OH)_2D$ to $1,24,25(OH)_3D$ in their fetuses, by increasing the expression of *Cyp24a1* in their placentas. We cannot exclude other possibilities such that the disturbance of 25OHD and $1,25(OH)_2D$ transport via placenta might contribute to the lower levels of 25OHD and $1,25(OH)_2D$ in the fetuses of *Hyp* mothers. In addition, it is also possible that the high fetal FGF23 in *Hyp* fetuses might have some roles in the regulation of fetal $1,25(OH)_2D$ levels by altering the gene expression in fetal kidney because the $1,25(OH)_2D$ level in *Hyp* fetuses was lower than that in their WT littermates (Fig. 7*H*).

Despite the increased FGF23 level in *Hyp* mothers, the level in their WT fetuses was as low as that in fetuses from WT mothers (Fig. 3*B*, *C*). These results suggest that maternal FGF23 is not transferred to the fetal circulation through the placenta. Alternatively, FGF23 may be rapidly degraded after placental transfer. Takaiwa and colleagues reported that a C-terminal fragment of FGF23 produced by degradation was abundant in normal human cord blood despite the low level of full-length FGF23.[33] To test the possibility that the appropriately regulated cleavage of FGF23 may play a role in the regulation of *Cyp24a1* expression by FGF23 in placenta, we injected recombinant WT FGF23 into the placenta and observed similar effects as those of recombinant FGF23(R179Q) (data not shown). Thus, the cleavage of FGF23 is unlikely to influence its function in terms of the regulation of *Cyp24a1* expression in placenta.

In XLH patients, hypophosphatemia may not be detected at birth, resulting in difficulty with an early diagnosis.[34] In the current study, we found that the plasma levels of Pi in both *Hyp* fetuses and their WT littermates from hypophosphatemic *Hyp* mothers were comparable to those in WT fetuses from WT mothers (Fig. 2*C*, *D*), which is consistent with the observation in newborn babies of patients with XLH. We also found that the circulating level of FGF23 in *Hyp* mice was already elevated before birth. Although there was no significant difference in the Pi level in fetal plasma (Fig. 2*D*) and amniotic fluid (Fig. 4*E*) among these genotypes, the high FGF23 level in *Hyp* fetuses suggests that hypophosphatemia may emerge soon after birth. Measurement of FGF23 in cord blood may aid the early diagnosis of XLH.

The elevated feto-maternal gradient of Pi levels in *Hyp* pregnancy suggests increased materno-fetal Pi transport via the placenta (Supplemental Fig. S3). RT-PCR and real-time PCR analyses revealed that WT mouse and normal human placenta express type IIb (*Slc34a2/SLC34A2*) and type III (*Slc20a1/SLC20A1* and *Slc20a2/SLC20A2*) Na^+/Pi cotransporters and their expressions increase during the development of the mouse placenta (Supplemental Fig. S1). On the other hand, type IIa and IIc Na^+/Pi cotransporters (*Slc34a1/SLC34A1* and *Slc34a3/SLC34A3*), which are targets of FGF23 in the kidney, were not expressed in placentas (Supplemental Fig. S1*A*, *B*). The placental expression of *Slc34a2*, *Slc20a1*, and *Slc20a2* was not altered in *Hyp* pregnancies at the mRNA level (Supplemental Fig. S4), and we have not identified the precise mechanism responsible for the elevated feto-maternal Pi gradient. The protein expression and/or function of these transporters may be altered in *Hyp* pregnancies, but this remains to be elucidated. Although the administration of recombinant FGF23 to WT placentas resulted in the altered expression of *Cyp24a1* and *Egr-1* within 30 minutes, there was no change in the Na^+-dependent uptake of Pi by placental membrane vesicles, which was probably mediated by a type IIb Na^+/Pi cotransporter (Supplemental Fig. S5*A*, *B*). These results suggest that FGF23 is unlikely to be implicated in the direct regulation of placental Pi transport. Some FGF23-independent mechanisms and/or unknown Pi transporters may play a role in the regulation of materno-fetal Pi transport.

In conclusion, the present study has shown that FGF23 exerts direct effects on the placenta and regulates the placental expression of *Cyp24a1* in pathological conditions with elevated FGF23 levels, including *Hyp* mice. It has also been revealed that an increased level of FGF23 in *Hyp* mice emerges before birth and is associated with altered gene expression in the fetal kidneys and placentas. These findings indicate the importance of the perinatal diagnosis of patients with XLH for their management.

Disclosures

All authors state that they have no conflicts of interest.

Acknowledgments

We thank Shoko Ikeda for her technical assistance in the ^{32}P uptake assay. We also thank Drs Akihiro Imura, Yo-ichi Nabeshima, Hiroyuki Tanaka, and Hiroki Kondou for their helpful discussions.

This work was supported in part by grants-in-aid for Scientific Research from the Ministry of Education, Science, and Culture, Japan, to TM; the Ministry of Health, Labour, and Welfare, Japan, to TM and KO; and funds from the Foundation of Growth Science to TM.

Authors' roles: Study design: YO, KO, and TM. Study conduct: KO and TM. Data collection: YO, MY, MK, NT, KT, TK, KM, AK, MN, and TM. Data analysis: YO, NT, and TM. Data interpretation: YO, MK, NT, NN, HY, TO, KO, and TM. Drafting manuscript: YO and TM. Revising manuscript content: YO, MK, NN, KO, and TM. Approving final version of manuscript: YO, MY, MK, NT, KT, TK, KM, AK, MN, NN, HY, TO, KO, and TM. YO and TM take responsibility for the integrity of the data analysis.

References

1. Quarles LD. Endocrine functions of bone in mineral metabolism regulation. J Clin Invest. 2008;118(12):3820–8.
2. Liu S, Zhou J, Tang W, et al. Pathogenic role of Fgf23 in Hyp mice. Am J Physiol Endocrinol Metab. 2006;291(1):E38–49.
3. Goetz R, Beenken A, Ibrahimi OA, et al. Molecular insights into the klotho-dependent, endocrine mode of action of fibroblast growth factor 19 subfamily members. Mol Cell Biol. 2007;27(9):3417–28.
4. Shimada T, Hasegawa H, Yamazaki Y, et al. FGF-23 is a potent regulator of vitamin D metabolism and phosphate homeostasis. J Bone Miner Res. 2004;19(3):429–35.
5. Shimada T, Kakitani M, Yamazaki Y, et al. Targeted ablation of Fgf23 demonstrates an essential physiological role of FGF23 in phosphate and vitamin D metabolism. J Clin Invest. 2004;113(4):561–8.
6. Segawa H, Kawakami E, Kaneko I, et al. Effect of hydrolysis-resistant FGF23-R179Q on dietary phosphate regulation of the renal type-II Na/Pi transporter. Pflugers Arch. 2003;446(5):585–92.
7. Carpenter TO. New perspectives on the biology and treatment of X-linked hypophosphatemic rickets. Pediatr Clin North Am. 1997;44(2):443–66.
8. A gene (PEX) with homologies to endopeptidases is mutated in patients with X-linked hypophosphatemic rickets. The HYP Consortium. Nat Genet. 1995;11(2):130–6.

9. Jonsson KB, Zahradnik R, Larsson T, et al. Fibroblast growth factor 23 in oncogenic osteomalacia and X-linked hypophosphatemia. N Engl J Med. 2003;348(17):1656–63.
10. Endo I, Fukumoto S, Ozono K, et al. Clinical usefulness of measurement of fibroblast growth factor 23 (FGF23) in hypophosphatemic patients: proposal of diagnostic criteria using FGF23 measurement. Bone. 2008;42(6):1235–9.
11. Beck L, Soumounou Y, Martel J, et al. Pex/PEX tissue distribution and evidence for a deletion in the 3' region of the Pex gene in X-linked hypophosphatemic mice. J Clin Invest. 1997;99(6):1200–9.
12. Sabbagh Y, Gauthier C, Tenenhouse HS. The X chromosome deletion in HYP mice extends into the intergenic region but does not include the SAT gene downstream from Phex. Cytogenet Genome Res. 2002;99(1–4):344–9.
13. Liu S, Tang W, Zhou J, et al. Fibroblast growth factor 23 is a counter-regulatory phosphaturic hormone for vitamin D. J Am Soc Nephrol. 2006;17(5):1305–15.
14. Boskey A, Frank A, Fujimoto Y, et al. The PHEX transgene corrects mineralization defects in 9-month-old hypophosphatemic mice. Calcif Tissue Int. 2009;84(2):126–37.
15. Kuro-o M, Matsumura Y, Aizawa H, et al. Mutation of the mouse klotho gene leads to a syndrome resembling ageing. Nature. 1997;390(6655):45–51.
16. Urakawa I, Yamazaki Y, Shimada T, et al. Klotho converts canonical FGF receptor into a specific receptor for FGF23. Nature. 2006; 444(7120):770–4.
17. Kurosu H, Ogawa Y, Miyoshi M, et al. Regulation of fibroblast growth factor-23 signaling by klotho. J Biol Chem. 2006;281(10):6120–3.
18. Liu S, Vierthaler L, Tang W, Zhou J, Quarles LD. FGFR3 and FGFR4 do not mediate renal effects of FGF23. J Am Soc Nephrol. 2008; 19(12):2342–50.
19. Gattineni J, Bates C, Twombley K, et al. FGF23 decreases renal NaPi-2a and NaPi-2c expression and induces hypophosphatemia in vivo predominantly via FGF receptor 1. Am J Physiol Renal Physiol. 2009; 297(2):F282–91.
20. Ben-Dov IZ, Galitzer H, Lavi-Moshayoff V, et al. The parathyroid is a target organ for FGF23 in rats. J Clin Invest. 2007;117(12):4003–8.
21. Krajisnik T, Bjorklund P, Marsell R, et al. Fibroblast growth factor-23 regulates parathyroid hormone and 1alpha-hydroxylase expression in cultured bovine parathyroid cells. J Endocrinol. 2007;195(1): 125–31.
22. Ohata Y, Arahori H, Namba N, et al. Circulating levels of soluble alpha-Klotho are markedly elevated in human umbilical cord blood. J Clin Endocrinol Metab. 2011;96(6):E943–7.
23. McClive PJ, Sinclair AH. Rapid DNA extraction and PCR-sexing of mouse embryos. Mol Reprod Dev. 2001;60(2):225–6.
24. Strom TM, Francis F, Lorenz B, et al. Pex gene deletions in Gy and Hyp mice provide mouse models for X-linked hypophosphatemia. Hum Mol Genet. 1997;6(2):165–71.
25. Kovacs CS, Manley NR, Moseley JM, Martin TJ, Kronenberg HM. Fetal parathyroids are not required to maintain placental calcium transport. J Clin Invest. 2001;107(8):1007–15.
26. Tsugawa N, Suhara Y, Kamao M, Okano T. Determination of 25-hydroxyvitamin D in human plasma using high-performance liquid chromatography-tandem mass spectrometry. Anal Chem. 2005; 77(9):3001–7.
27. Higashi T, Awada D, Shimada K. Simultaneous determination of 25-hydroxyvitamin D2 and 25-hydroxyvitamin D3 in human plasma by liquid chromatography-tandem mass spectrometry employing derivatization with a Cookson-type reagent. Biol Pharm Bull. 2001;24(7):738–43.
28. Tomiyama K, Maeda R, Urakawa I, et al. Relevant use of Klotho in FGF19 subfamily signaling system in vivo. Proc Natl Acad Sci USA. 2010;107(4):1666–71.
29. Watson ED, Cross JC. Development of structures and transport functions in the mouse placenta. Physiology (Bethesda). 2005; 20:180–93.
30. Kovacs CS, Woodland ML, Fudge NJ, Friel JK. The vitamin D receptor is not required for fetal mineral homeostasis or for the regulation of placental calcium transfer in mice. Am J Physiol Endocrinol Metab. 2005;289(1):E133–44.
31. Goetz R, Ohnishi M, Kir S, et al. Conversion of a paracrine fibroblast growth factor into an endocrine fibroblast growth factor. J Biol Chem. 2012;287(34):29134–46.
32. Rossant J, Cross JC. Placental development: lessons from mouse mutants. Nat Rev Genet. 2001;2(7):538–48.
33. Takaiwa M, Aya K, Miyai T, et al. Fibroblast growth factor 23 concentrations in healthy term infants during the early postpartum period. Bone. 2010;47(2):256–62.
34. Minamitani K, Minagawa M, Yasuda T, Niimi H. Early detection of infants with hypophosphatemic vitamin D resistant rickets (HDRR). Endocr J. 1996;43(3):339–43.

THE JOURNAL OF BIOLOGICAL CHEMISTRY VOL. 289, NO. 3, pp. 1457–1466, January 17, 2014

Sympathetic Activation Induces Skeletal *Fgf23* Expression in a Circadian Rhythm-dependent Manner*[S]

Received for publication, August 1, 2013, and in revised form, November 18, 2013 Published, JBC Papers in Press, December 3, 2013, DOI 10.1074/jbc.M113.500850

Masanobu Kawai[‡1], **Saori Kinoshita**[‡], **Shigeki Shimba**[§], **Keiichi Ozono**[¶], **and Toshimi Michigami**[‡]

From the [‡]*Department of Bone and Mineral Research, Osaka Medical Center and Research Institute for Maternal and Child Health, 840 Murodo-cho, Izumi, Osaka 594-1101, Japan, the* [§]*Department of Health Science, School of Pharmacy, Nihon University, 7-7-1 Narashinodai, Funabashi, Chiba 274-8555, Japan, and the* [¶]*Department of Pediatrics, Osaka University Graduate School of Medicine, 2-2 Yamadaoka, Suita, Osaka 565-0871, Japan*

Background: The mechanism whereby the circadian clock regulates phosphate metabolism remains elusive.
Results: *Fgf23* expression is regulated by the time of food intake which involves the alteration in circadian profile of sympathetic activity.
Conclusion: The circadian network plays important roles in phosphate metabolism.
Significance: The sympathetic regulation of *Fgf23* expression may shed light on new regulatory networks that could be important for phosphate homeostasis.

The circadian clock network is well known to link food intake and metabolic outputs. Phosphorus is a pivotal nutritional factor involved in energy and skeletal metabolisms and possesses a circadian profile in the circulation; however, the precise mechanisms whereby phosphate metabolism is regulated by the circadian clock network remain largely unknown. Because sympathetic tone, which displays a circadian profile, is activated by food intake, we tested the hypothesis that phosphate metabolism was regulated by the circadian clock network through the modification of food intake-associated sympathetic activation. Skeletal *Fgf23* expression showed higher expression during the dark phase (DP) associated with elevated circulating FGF23 levels and enhanced phosphate excretion in the urine. The peaks in skeletal *Fgf23* expression and urine epinephrine levels, a marker for sympathetic tone, shifted from DP to the light phase (LP) when mice were fed during LP. Interestingly, β-adrenergic agonist, isoproterenol (ISO), induced skeletal *Fgf23* expression when administered at ZT12, but this was not observed in *Bmal1*-deficient mice. *In vitro* reporter assays revealed that ISO trans-activated *Fgf23* promoter through a cAMP responsive element in osteoblastic UMR-106 cells. The mechanism of circadian regulation of *Fgf23* induction by ISO *in vivo* was partly explained by the suppressive effect of Cryptochrome1 (Cry1) on ISO signaling. These results indicate that the regulation of skeletal *Fgf23* expression by sympathetic activity is dependent on the circadian clock system and may shed light on new regulatory networks of FGF23 that could be important for understanding the physiology of phosphate metabolism.

Phosphorus is an indispensable nutritional element involved in numerous biological processes such as cell signaling, energy homeostasis, and bone metabolism (1–4). The regulation of phosphate metabolism is an integrated process involving multiple organs and accumulating evidence has demonstrated the pivotal roles of fibroblast growth factor 23 (FGF23)[2] in phosphate metabolism (4–9). FGF23 is produced mainly by osteoblastic cells, including osteocytes, and functions as an endocrine factor to regulate genes involved in phosphate and vitamin D metabolism (4). The nodal point of the regulation of phosphate metabolism by FGF23 seems to primarily reside in the suppression of NaP_i-IIa/c expression and 1,25-dihydroxyvitamin D production in the kidney (4). Clinical evidence from genetic disorders in which mutations in the *FGF23* gene or mutations causing aberrant FGF23 signaling are associated with dysregulated phosphate metabolism has placed bone-derived FGF23 in the center of regulatory networks of phosphate metabolism (10–12). Hence, it is critical to understand the mode of the regulation of FGF23 expression in the skeleton to fully understand the physiological and pathological functions of FGF23 in phosphate metabolism. Although previous studies have revealed that 1,25-dihydroxyvitamin D can stimulate *Fgf23* expression in bone in part by directly activating the *Fgf23* gene promoter (13–15), the precise mechanisms by which skeletal *Fgf23* expression is regulated remain largely elusive. Because serum phosphate levels have been shown to exhibit circadian profile in humans, it is likely that phosphate metabolism is under the regulation of the circadian clock system (16–18); however, the precise mechanism by which the circadian clock network regulates phosphate homeostasis is still largely unknown.

The circadian clock network is an evolutionarily conserved process by which organisms adapt to environmental cues such as the availability of nutrients (19–21). For example, when food access is restricted in mice in the daytime (light phase) only, the expression profiles of circadian clock genes and circadian-reg-

* This work was supported by a grant from Sukoyaka Grant for Maternal and Child Health (to M. K.).
[S] This article contains supplemental Figs. S1 and S2.
[1] To whom correspondence should be addressed. Tel.: 81-725-56-1220; Fax: 81-725-57-3021; E-mail: kawaim@mch.pref.osaka.jp.

[2] The abbreviations used are: FGF23, fibroblast growth factor 23; AL, *ad libitum*; CRE, cAMP responsive element; CREB, CRE-binding protein; DP, dark phase; IBMX, 3-isobutyl-1-methylxanthine; ISO, isoproterenol; LP, light phase; PRO, propranolol; PTH, parathyroid hormone; RF, restricted feeding; ZT, zeitgeber time.

TABLE 1
Primer sequences for real-time RT-PCR

Gene	Forward Primer	Reverse Primer
Rev-erbα	5′-cccaacgacaacaacctttg-3′	5′-ccctggcgtagaccattcag-3′
Dbp	5′-caccgtggaggtgctaatga-3′	5′-gcttgacagggcgagatca-3′
Bmal1	5′-aggcccacagtcagattgaaa-3′	5′-ccaaagaagccaattcatcaatg-3′

ulated genes related to metabolic outputs have been shown to exhibit a phase shift so that the organisms can utilize ingested nutrients in a timely manner (19, 22–24). The central pacemaker of the circadian clock system is located at the suprachiasmatic nucleus in the hypothalamus and is integrated by multiple steps including transcriptional, translational, and post-translational mechanisms (20). Briefly, Clock (circadian locomotor output cycles protein kaput) heterodimerizes with Bmal1 (brain and muscle ARNT-like 1; also known as ARNTL) and induces the expression of *PER* (period circadian protein) and *CRY* (cryptochrome), which in turn suppresses Clock/Bmal1 transcriptional activity, thereby forming a 24-h feedback loop (20).

The mechanisms by which nutrient availability affects the circadian clock network still need to be determined; however both central and peripheral networks have been implicated as functional in this regulation (20). Centrally, the food-entrainable oscillator, which is anatomically different from the suprachiasmatic nucleus, has been considered to determine food-anticipatory behavior (20). Changes in the circadian profile of sympathetic activity may be one of the central mechanisms connecting food intake and metabolic outputs because food intake has been shown to be associated with enhanced sympathetic activity (25–28). In addition to central regulation, peripheral tissues also possess an oscillator that is synchronized with the central circadian system through retinal, hormonal, nutritional, and neuronal signals (29, 30). Recent advances in our understanding regarding the role of the peripheral oscillator have emphasized its importance in metabolic regulation (21). Furthermore, it has been well established that the circadian clock system in peripheral tissues is entrained by nutritional cues (21, 23). Taken together, these findings led us to hypothesize that phosphate metabolism was regulated by the circadian clock network through the modification of food intake-associated sympathetic activation, which may involve the action of the peripheral clock system.

In the current study, we tested our hypothesis that the circadian profile of circulating phosphate and FGF23 levels is determined by the time of nutrient availability by analyzing the circadian profile of skeletal *Fgf23* expression in mice where the timing of food intake was restricted during the light phase and found that light phase-restricted feeding altered the circadian expression profile of skeletal *Fgf23*, which was in part caused by changes in the circadian profile of sympathetic activity. In addition, we demonstrated that stimulation with a β-adrenergic receptor agonist induced *Fgf23* expression, which was suppressed by the overexpression of Cry1. These results underline the important roles of the circadian clock system in the regulation of phosphate metabolism.

EXPERIMENTAL PROCEDURES

Mice—C57BL/6J mice were purchased from CLEA Japan, Inc., and *Bmal1* knock-out mice on a C57BL/6J background were generated as reported previously (31). Mice were maintained on a 12-h:12-h light dark cycle (lights on at zeitgeber time (ZT) 0) in a pathogen-free animal facility with free access to water and standard chow (CE-2; CLEA Japan, Inc.), unless otherwise mentioned. The light phase restricted feeding regimen was carried out by allowing mice access to food for 6 h between ZT2 and ZT8. A control diet containing 0.6% phosphate and 1.0% calcium and a high phosphate diet containing 1.65% phosphate and 1.0% calcium were purchased from CLEA Japan, Inc. All animal studies were reviewed and approved by the Institutional Animal Care and Use Committee of Osaka Medical Center and Research Institute for Maternal and Child Health.

Reagents and Cell Lines—Isoproterenol hydrochloride, propranolol hydrochloride, and 3-isobutyl-1-methylxanthine (IBMX) were purchased from Wako Pure Chemical Industries Ltd. (Osaka, Japan). Human parathyroid hormone (PTH)(1–34) was obtained from the Peptide Institute, Inc. (Osaka, Japan). UMR-106 cells were obtained from ATCC (Manassas, VA) and maintained in DMEM supplemented with 10% fetal bovine serum and 1% insulin-transferrin-selenium-G supplement (Invitrogen). Cells were cultured at 37 °C in a 5% CO_2 atmosphere.

Real-time RT-PCR—Total RNA was prepared using TRIzol (Invitrogen) and treated with DNase I (Qiagen). cDNA was generated using a random hexamer and reverse transcriptase (Superscript II; Invitrogen) according to the manufacturer's instructions. The quantification of mRNA expression was carried out using a 7300 Real-time PCR system or a StepOnePlus™ Real-time PCR system (Applied Biosystems). TaqMan Gene Expression Assays for *Fgf23*, *Cryptochrome1*, *Rankl*, *Sost*, *Slc34a1*, *Slc34a3*, *Cyp27b1*, *Cyp24a1*, and *Gapdh* were purchased from Applied Biosystems. Primer sequences for *Rev-erbα*, *Dbp*, and *Bmal1* are described in Table 1. *Gapdh* was used as an internal standard control gene for all quantifications.

Western Blot Analysis—To prepare whole cell lysates, cells were solubilized in radioimmunoprecipitation assay buffer (1% Triton X-100, 1% sodium deoxycholate, 0.1% SDS, 150 mM NaCl, 10 mM Tris-Cl (pH 7.4), 5 mM EDTA, 1 mM orthovanadate, and protease inhibitor mixture (Complete™; Roche Diagnostics). Equal amounts of protein were separated by SDS-PAGE and transferred electrophoretically to PVDF membranes. Membranes were blocked in BlockAce reagent (Dainippon Pharmaceuticals, Osaka, Japan) or Blocking-one P reagent (Nacalai Tesque, Kyoto, Japan), immunoblotted with anti-CREB (1:1000, 9192; Cell Signaling, Beverly, MA), anti-pCREB (1:1000, 9191; Cell Signaling), anti-V5 (1:5000, 46-0705; Invitrogen), or anti-β-actin (1:2000, sc-47778; Santa Cruz Bio-

technology) and developed with horseradish peroxidase-coupled secondary antibodies, followed by enhancement with a chemiluminescence (ECL) detection system (GE Healthcare).

Generation of Adenoviruses—Adenoviruses carrying GFP or Cry1 were constructed using the ViraPower Adenoviral Expression System (Invitrogen). Briefly, cDNA was inserted into a TOPO pENTR vector and was recombined to the adenovirus expression plasmid pAd/CMV/V5-DEST. The pAd/CMV/V5-DEST plasmid with the cDNA of interest was digested with the PacI endonuclease and transfected with HEK293A cells. The medium supernatant containing the adenovirus was collected and titrated according to the manufacturer's instructions. UMR-106 cells were infected with the adenovirus at a multiplicity of infection of 500 with 4 μg/ml poly-L-lysine (Sigma).

Constructs and Luciferase Reporter Assay—The Cry1 expression construct with a V5 tag was created by subcloning the corresponding PCR products into the pENTR vector using the pENTR Directional TOPO cloning kit (Invitrogen) and transferring to the pcDNA3.2/V5 vectors using the LR recombination reaction system (Invitrogen). Luciferase vectors containing 2000 bp of the mouse *Fgf23* gene promoter (−1872 to +128) (2000bp-Luc) was prepared by subcloning the corresponding PCR products into pGL4.20[luc2/Puro] (Promega, Madison, WI) vectors according to the previous report (13). Luciferase constructs containing 766 bp (−638 to +128) of the *Fgf23* gene promoter were created by the digestion of 2000bp-Luc with BglII (located at the 5′ region in the multiple cloning site of the pGL4.20 vector relative to the insert and −638 to −633) followed by the ligation of fragments containing luciferase with T4 DNA ligase. Luciferase constructs containing 143 bp (−15 to +128) of the *Fgf23* gene promoter were designed by digesting pT7 vectors harboring 2000 bp of the *Fgf23* gene promoter with SmaI (located at −18 to −13 and the 3′ region in the pT7 vector relative to the insert) followed by the ligation of fragments containing the promoter region of interest with pGL4.20[luc2/Puro] vectors digested with EcoRV using T4 DNA ligase.

Mutagenesis—Two candidate motifs were detected as possible cAMP responsive elements (CREs) in the promoter region of the *Fgf23* gene by *in silico* analysis, and these motifs were designated as CRE1 and CRE2, respectively. To determine whether these motifs were functional, site-directed mutagenesis was performed using QuikChange II XL (Agilent Technologies, Santa Clara, CA) according to the manufacturer's protocol. The CRE1 located at −620 to −613 and CRE2 located at −46 to −39 were mutated from TGACCTCA to TGAAATCA and TGATGTCA to TGAAATCA, respectively.

Luciferase Assay—UMR-106 cells were seeded in a 24-well plate at a density of 5×10^4 cells/well, and transient transfection was carried out using FuGENE HD (Promega) following the manufacturer's protocol. The total amount of DNA added to each well was equalized using an empty vector. The luciferase assay was performed in triplicate according to the protocol of the dual-luciferase reporter assay system (Promega). Briefly, 24 h after transfection cells were treated with isoproterenol (10 or 100 μM) and/or IBMX (0.5 mM) in DMEM containing 1% FCS overnight, followed by the determination of luciferase activity using specific substrates in a luminometer. Transfection efficiency was normalized by co-transfection with the TK-*Renilla* luciferase construct (Promega). While Cry1-overexpressing UMR-106 cells were used for the luciferase assay, UMR-106 cells were infected with an adenovirus containing GFP or Cry1-V5. Twenty-four h after the infection cells were trypsinized and plated in a 24-well plate as described above.

Animal Studies—Isoproterenol or PTH(1–34) was dissolved in saline and administered intraperitoneally at a dose of 6 μg/g (32) or 100 μg/kg, respectively. A saline injection was used as a control treatment. Whereas propranolol (PRO) was used for the *in vivo* study, PRO was dissolved in the drinking water at a concentration of 0.5 g/liter (33), and the drinking water was changed three times a week.

Measurement of Serum and Urine Parameters—The measurement of serum phosphate was carried out using P-test Wako (Wako Pure Chemical Industries Ltd., Osaka, Japan). Total (C-Term) and intact (full-length) FGF23 concentrations were determined by ELISA from Immutopics, Inc., San Clemente, CA and Kainos Laboratory, Tokyo, Japan, respectively, following the manufacturers' instructions. Urine samples were collected in the presence of 5 μl of 5 N HCl, and the volume of urine was measured. Urine epinephrine was determined using ELISA (IBL, Hamburg, Germany). Urine phosphate and creatinine were measured using P-test Wako and Creatinine Test Kit (Wako Pure Chemical Industries Ltd.), respectively.

Statistical Analysis—All data are expressed as the mean ± S.E. Results were examined for significant differences using Student's *t* test or analysis of variance followed by the Bonferroni multiple comparison *post hoc* test. Significance was set at $p < 0.05$.

RESULTS

Skeletal Fgf23 Exhibited a Circadian Expression Profile—To investigate the mechanisms whereby phosphate metabolism is regulated by the circadian clock network, we first examined the circadian expression profile of *Fgf23* in the femur of wild-type mice fed standard chow *ad libitum* (AL). As reported previously (34), components of the clock network including *Rev-erbα* (nuclear receptor subfamily 1, group D, member 1; Nr1d1), *Dbp* (D site of albumin-binding protein), and *Cry1* exhibited rhythmic expression patterns in the femur (Fig. 1, *A–C*, and supplemental Fig. S1). The *Fgf23* expression profile showed higher expression levels during the dark phase (DP) compared with the light phase (LP) with the highest at ZT16 (Fig. 1*D* and supplemental Fig. S1). Because it is well known that food consumption reaches highest at the beginning of DP in mice fed AL, we speculated that skeletal *Fgf23* expression was regulated by the food consumption in a manner involving the circadian clock system. To test this speculation, mice were fed during the LP from ZT2 to ZT8 (LP-restricted feeding: LP-RF) for 10 days. Because it is unclear whether skeletal tissue is entrained by nutrient availability despite the fact that food intake is a strong zeitgeber in peripheral tissues such as liver, we examined the circadian expression profiles of genes involved in daily oscillations in the femur. As shown in Fig. 2, *A–C*, and supplemental Fig. S2, the peak expressions of *Rev-erbα*, *Dbp*, and *Cry1* shifted by 12 h in mice under LP-RF conditions compared with AL conditions, suggesting that skeletal tissue is also

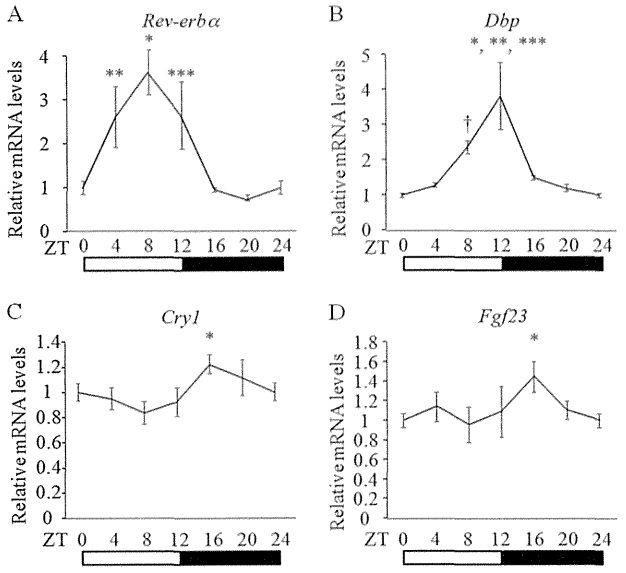

FIGURE 1. **Fgf23 showed a rhythmic expression pattern in the femur of mice fed *ad libitum*.** WT mice were maintained under a light-dark regimen (12-h:12-h cycle) and fed *ad libitum*. Samples were collected every 4 h from ZT0. *A*, expression of *Rev-erbα* ($n = 3$–4, *, $p < 0.01$ *versus* ZT0 and ZT20; **, $p < 0.05$ *versus* ZT20; ***, $p < 0.05$ *versus* ZT0, ZT16 and ZT20). *B*, expression of *Dbp* ($n = 3$, *, $p < 0.001$ *versus* ZT0, ZT4, and ZT20; **, $p < 0.01$ *versus* ZT16; ***, $p < 0.05$ *versus* ZT8; †, $p < 0.05$ *versus* ZT0). *C*, expression of *Cry1* ($n = 5$–7, *, $p < 0.05$ *versus* ZT8). *D*, expression of *Fgf23* ($n = 5$–7, *, $p < 0.05$ *versus* ZT8). All expression was in the femur and was analyzed using real-time RT-PCR. The *white bar* and *black bar* represent the light phase and dark phase, respectively. Values are expressed as the mean ± S.E. (*error bars*).

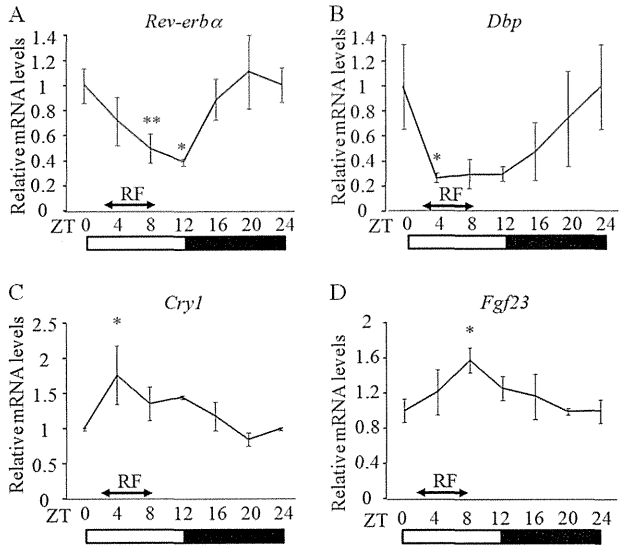

FIGURE 2. **Light phase restricted feeding altered the expression profile of *Fgf23* in the femur.** WT mice were maintained under a light-dark regimen (12-h:12-h cycle) and fed for 6 h from ZT2 to ZT8 for 10 days. Samples were collected every 4 h from ZT0. *A*, expression of *Rev-erbα* ($n = 3$, *, $p < 0.05$ *versus* ZT0 and ZT20; **, $p < 0.05$ *versus* ZT20). *B*, expression of *Dbp* ($n = 3$, *, $p < 0.05$ *versus* ZT0). *C*, expression of *Cry1* ($n = 3$–4, *, $p < 0.05$ *versus* ZT0 and ZT20). *D*, expression of *Fgf23* ($n = 3$, *, $p < 0.05$ *versus* ZT0). All expression was in the femur and was determined by real-time RT-PCR. The *white bar* and *black bar* represent the light phase and dark phase, respectively. Values are expressed as the mean ± S.E. (*error bars*).

entrained by nutrient availability. Based on this observation, we next analyzed the expression profile of *Fgf23* in the femur and found that *Fgf23* showed a rhythmic expression pattern with a peak expression at ZT8 (Fig. 2*D* and supplemental Fig. S2). Taken together, these findings indicate that *Fgf23* expression

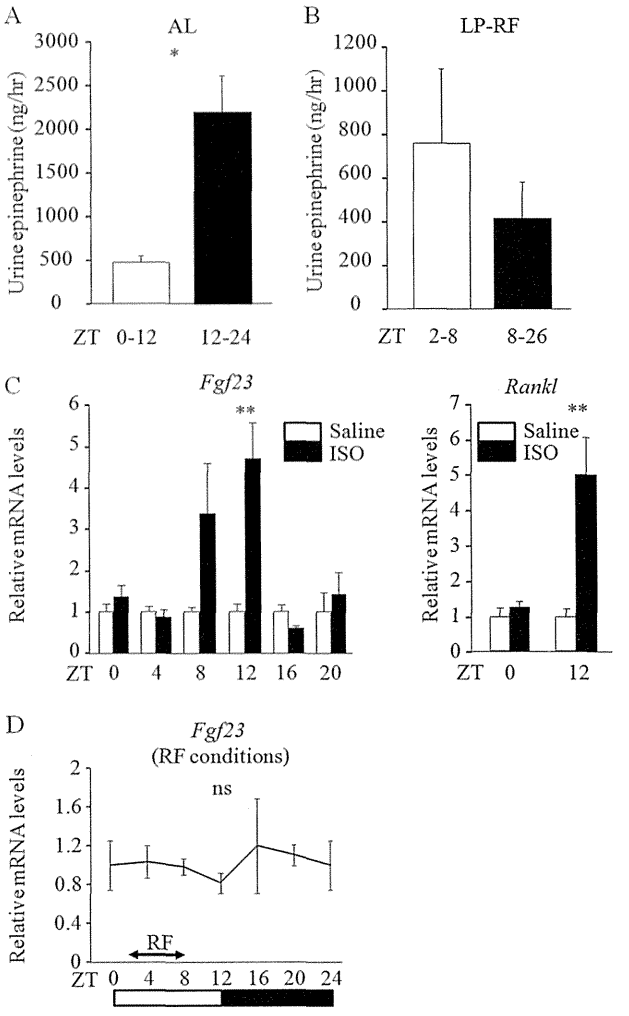

FIGURE 3. **Sympathetic activation induced skeletal *Fgf23* expression *in vivo*.** *A*, urine was collected from WT mice under *ad libitum* (*AL*) conditions either during the light phase (LP: ZT0–12) or the dark phase (ZT12–24). The volume of urine and urine epinephrine levels were measured, and the amount of urine epinephrine/h was determined ($n = 9$). *B*, urine was collected from WT mice under LP-RF conditions either during ZT2–8 or ZT8–26. The volume of urine and urine epinephrine levels were measured, and the amount of urine epinephrine/h was determined ($n = 7$). *C*, ISO was administered intraperitoneally to WT mice under AL conditions at different time points of the day as indicated, and 4 h after the injection the expression of *Fgf23* and *Rankl* in the femur was determined by real-time RT-PCR ($n = 3$–4). *D*, WT mice were maintained under LP-RF conditions for 10 days, and 0.5 g/liter propranolol was added to the drinking water from day 7 to day 10. Femurs were collected at indicated time points, and *Fgf23* expression was measured by real-time RT-PCR ($n = 3$). The *white bar* and *black bar* represent the light phase and dark phase, respectively. *ns*, not significantly different. Values are expressed as the mean ± S.E. (*error bars*). *, $p < 0.001$; **, $p < 0.05$.

possesses a circadian expression profile that is at least in part determined by the time of nutrient availability.

Sympathetic Activation Enhanced Fgf23 Expression in the Femur—It is well known that food intake is tightly coupled to an increase in the metabolic rate to adjust for the increase in nutrient influx, which in part involves an elevation in sympathetic activity (25–28). Indeed, urine levels of epinephrine, a marker for sympathetic activity, in mice fed AL were significantly enhanced in DP compared with LP (Fig. 3*A*). Interestingly, LP-RF caused a phase shift in sympathetic activity with greater levels during LP-RF, but the difference did not reach statistical significance (Fig. 3*B*). Based on these findings, we speculated

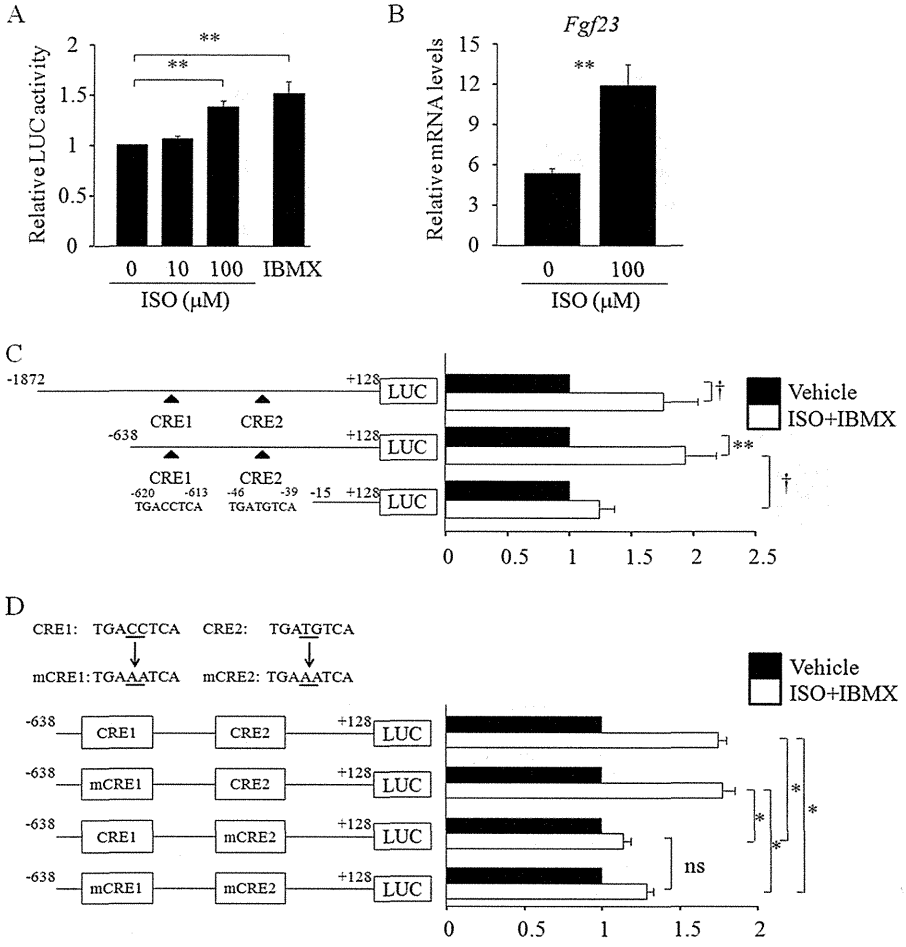

FIGURE 4. **ISO trans-activated *Fgf23* transcription in UMR-106 cells.** *A*, UMR-106 cells were seeded in 24-well plates and transfected with 2000bp-Luc (200 ng) and phRL-TK (10 ng). Twenty-four h after transfection, cells were treated with ISO at a dose of 10 or 100 μM overnight, and luciferase activity was measured. 0.5 mM IBMX was used as a positive control for the activation of cAMP signaling ($n = 3$). *B*, UMR-106 cells were treated with 100 μM ISO overnight, and expression of *Fgf23* was determined by real-time RT-PCR ($n = 4$). *C*, UMR-106 cells were seeded in 24-well plates and transfected with 2000bp-Luc (200 ng), 766bp-Luc (200 ng), or 143bp-Luc (200 ng) and phRL-TK (10 ng). Twenty-four h after transfection, cells were treated with ISO (100 μM) and IBMX (0.5 mM) overnight, and luciferase activity was measured ($n = 5$). *D*, UMR-106 cells were seeded in 24-well plates and transfected with 766bp-Luc (200 ng) or 766bp-Luc containing mutations in CRE1 and/or CRE2 (200 ng), and phRL-TK (10 ng). Twenty-four h after transfection, cells were treated with ISO (100 μM) and IBMX (0.5 mM) overnight, and luciferase activity was measured ($n = 4$). Values are expressed as the mean ± S.E. (*error bars*). *ns*, not significantly different. *, $p < 0.001$; **, $p < 0.01$; †, $p < 0.05$.

that *Fgf23* expression may at least in part be regulated by sympathetic activation in a circadian manner. To test this idea, we intraperitoneally administered the β-adrenergic receptor agonist, isoproterenol (ISO), to mice at different time points of the day and analyzed the expression of *Fgf23* in the femur 4 h after the injection. The administration of ISO caused an increase in skeletal *Fgf23* expression when injected at ZT8 ($p = 0.12$) and ZT12 ($p < 0.05$), whereas ISO treatment had no effect on *Fgf23* expression when administered at the other time points (Fig. 3*C*). To determine whether the effect of ISO was specific to *Fgf23* induction, we also analyzed the expression of *Rankl*, one of the target genes of ISO (35), and found that the induction of *Rankl* showed a pattern similar to that of *Fgf23* induction (Fig. 3*C*). To further understand the involvement of sympathetic activity in the circadian *Fgf23* profile, mice were maintained under LP-RF in the presence of the β-blocker, PRO, to analyze the effect of sympathetic activity on the peak expression of *Fgf23* noted at ZT8. Interestingly, *Fgf23* expression did not exhibit any circadian profile when PRO was concomitantly administered, indicating the involvement of sympathetic activity in the circadian profile of *Fgf23* expression in the femur (compare Fig. 3*D* with Fig. 2*D*, and see supplemental Fig. S2).

ISO Trans-activated the Fgf23 Gene Promoter and Induced Fgf23 Expression in UMR-106 Cells—Because *in vivo* administration of ISO enhanced the expression of *Fgf23* in the femur, we investigated whether ISO signaling trans-activated *Fgf23* gene promoter using osteoblastic UMR-106 cells in which endogenous *Fgf23* was expressed. For this purpose, we generated a luciferase construct containing a 2000-bp promoter region of the mouse *Fgf23* gene. The treatment with ISO showed a significant increase in luciferase activity in a dose-dependent manner (Fig. 4*A*). In line with this, the ISO treatment enhanced the expression of *Fgf23* in these cells (Fig. 4*B*). These results suggest that ISO induces *Fgf23* expression at least in part by activating the transcription of the *Fgf23* gene. Because *in silico* analysis pointed out the existence of two motifs whose sequences were very similar to CRE, we next tested whether these motifs, designated as CRE1 and CRE2, respectively, were involved in ISO-induced *Fgf23* trans-activation. For this purpose, we generated luciferase vectors containing the truncated

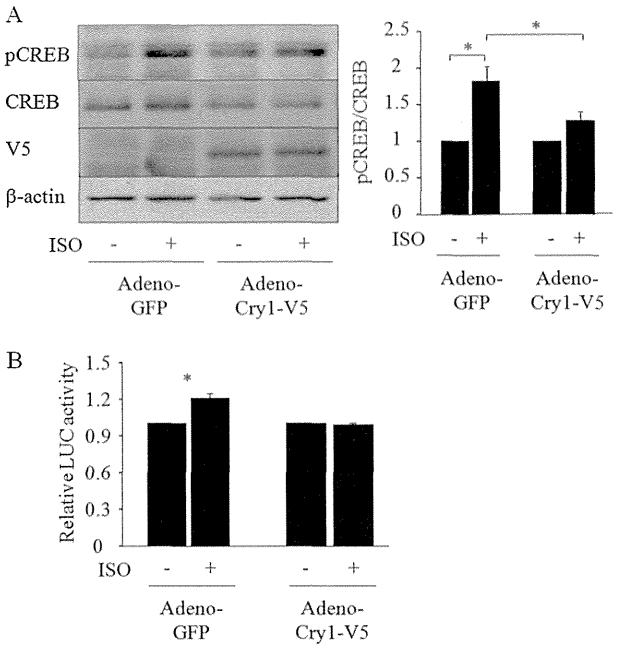

FIGURE 5. **Cry1 suppressed ISO-induced phosphorylation of CREB in UMR-106 cells.** *A*, UMR-106 cells were infected with an adenovirus containing GFP or Cry1-V5 and treated with 100 μM ISO for 5 min. The expression of pCREB, CREB, V5, and β-actin was determined by Western blotting, and expression of pCREB was quantified by normalizing to the levels of CREB by densitometric analysis ($n = 5$). *B*, UMR-106 cells infected with an adenovirus containing either GFP or Cry1 were seeded in 24-well plates and transfected with 2000bp-Luc (200 ng) and phRL-TK (10 ng). Twenty-four h after transfection cells were treated with 100 μM ISO overnight, and luciferase activity was measured ($n = 3$). The figures shown are the representative from at least three independent experiments. Values are expressed as the mean ± S.E. (*error bars*). *, $p < 0.05$.

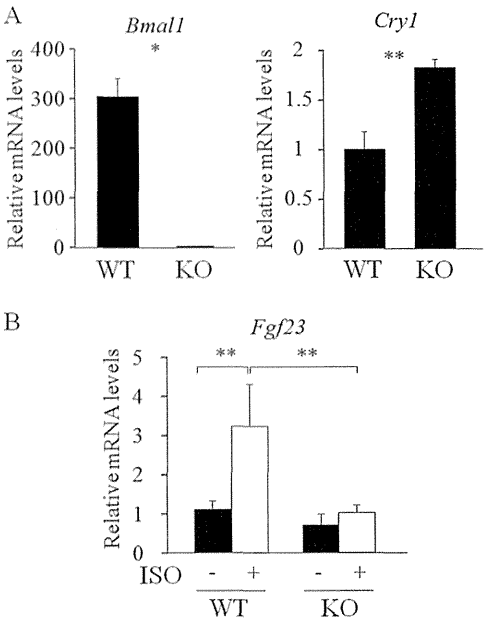

FIGURE 6. **Fgf23 induction by the ISO treatment in the femur was impaired in *Bmal1*-deficient mice.** *A*, the expression of *Bmal1* and *Cry1* was determined by real-time RT-PCR in the femur collected from WT mice and *Bmal1*-deficient mice at ZT16 ($n = 3–5$). *B*, WT mice and *Bmal1*-deficient mice were fed a control diet for 2 weeks from 8 weeks of age, and ISO was injected intraperitoneally at ZT12. Four h after the injection, the expression of *Fgf23* in the femur was analyzed by real-time RT-PCR ($n = 4–5$). Values are expressed as the mean ± S.E. (*error bars*). *, $p < 0.01$; **, $p < 0.05$.

forms of the *Fgf23* gene promoter and found that the luciferase vectors containing CRE1 and CRE2 were responsive to the ISO/IBMX treatment (Fig. 4*C*). To determine the responsible motif(s) for this trans-activation of the *Fgf23* gene promoter, we introduced mutations in CRE1 and/or CRE2 and found that CRE2 was responsible for ISO/IBMX-induced activation of the *Fgf23* gene promoter (Fig. 4*D*).

Overexpression of Cry1 Blunted the Effects of ISO on Fgf23 Induction in UMR-106 Cells—These findings may support the concept that *Fgf23* expression is regulated by sympathetic activity, but it is still unclear as to why *Fgf23* induction by ISO is regulated in a time-dependent manner *in vivo*. To solve this issue, we assessed whether Cry1 was involved in the ISO-induced activation of *Fgf23* expression because Cry1 has been implicated in the suppression of ISO-induced cAMP accumulation in HEK293 cells (36). Indeed, ISO-induced *Fgf23* expression was evident when Cry1 expression was low in the femur (Figs. 1*C* and 3*C*). Based on these results, we tested our hypothesis that Cry1 suppressed ISO-induced *Fgf23* induction by blocking CREB signaling in osteoblastic cells. To test this hypothesis, we overexpressed Cry1 in UMR-106 cells and investigated the effect of ISO on the phosphorylation of CREB. As shown in Fig. 5*A*, the ISO-induced phosphorylation of CREB was impaired in Cry1-overexpressing cells compared with GFP-expressing control cells. In line with this, ISO-induced trans-activation of the *Fgf23* promoter was decreased in cells overexpressing Cry1 (Fig. 5*B*). To further determine the role of the circadian clock network in ISO-induced *Fgf23* induction, we utilized *Bmal1*-deficient mice in which *Cry1* expression was higher than that in WT littermate controls (Fig. 6*A*). The administration of ISO at ZT12 showed a significant increase in *Fgf23* expression in the femur of WT mice, whereas the induction of *Fgf23* was weaker in the femur of *Bmal1*-deficient mice (Fig. 6*B*).

Parathyroid Hormone Induced Fgf23 Expression When Administered at ZT12—Because PTH has been shown to activate the CREB pathway and induce *Fgf23* expression (4, 37), we next tested whether the PTH-induced activation of *Fgf23* was also regulated in a circadian rhythm-dependent manner. To test this hypothesis, we administered PTH(1–34) intraperitoneally to WT mice at ZT0 or ZT12. Four h after the injection, the expression of *Fgf23* was analyzed in the femur. The skeletal expression of *Fgf23* exhibited a significant response to PTH when injected at ZT12, which was associated with a trend toward an increased expression of *Rankl* and a decreased expression of *Sost*, known to be regulated by PTH activation in osteoblastic cells (38), whereas PTH had no effect on *Fgf23* expression when injected at ZT0 (Fig. 7). These results suggest the possibility of the circadian regulation of PTH action with respect to *Fgf23* induction in the skeleton.

Fgf23 Induction by Dietary Phosphate Load Was Not Likely Caused by Sympathetic Activation—Because it is still unclear as to whether circadian *Fgf23* expression is regulated by food intake itself or the influx of phosphate from the diet, we finally tested whether sympathetic activity was involved in *Fgf23* induction by dietary phosphate load. For this purpose, WT mice were fed either a control diet or high phosphate diet for 2 weeks in the presence or absence of PRO. Ingesting the high

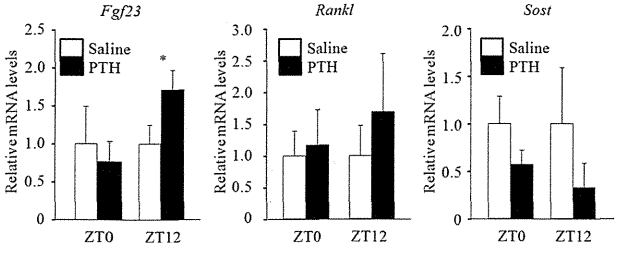

FIGURE 7. **PTH induced skeletal *Fgf23* expression in a circadian fashion.** PTH was intraperitoneally administered in WT mice at ZT0 or ZT12, and samples were collected 4 h after the injection. The expression of *Fgf23*, *Rankl*, and *Sost* in the femur was determined using real-time RT-PCR (n = 3–6). Values are expressed as the mean ± S.E. (*error bars*). *, $p < 0.05$.

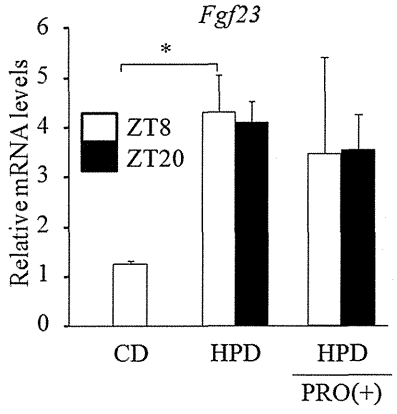

FIGURE 8. **Propranolol did not affect skeletal *Fgf23* expression induced by dietary phosphate load.** WT mice were fed either control diet (*CD*) or high phosphate diet (*HPD*) for 2 weeks from 8 weeks of age in the presence or absence of PRO in the drinking water. The expression of *Fgf23* in the femur was determined using real-time RT-PCR (n = 3–5). Values are expressed as the mean ± S.E. (*error bars*). *, $p < 0.01$.

phosphate diet caused a significant elevation in *Fgf23* expression in the femur (Fig. 8), but the concomitant administration of PRO did not affect the levels of *Fgf23* expression in the femur (Fig. 8), which indicates that the timing of food intake, and not the amount of ingested phosphate, may determine the circadian profiles of skeletal *Fgf23* expression.

The Increase in Skeletal Fgf23 Expression during DP Was Associated with Elevated FGF23 Levels in Serum and Enhanced Phosphate Excretion in the Urine—We finally investigated the association between the increase in skeletal *Fgf23* expression during DP and systemic phosphate metabolism. Consistent with the rhythmic expression pattern of skeletal *Fgf23*, total FGF23 levels in the serum exhibited a circadian expression profile with peak levels at ZT 16 (Fig. 9*A*). Circulating biologically active (intact) FGF23 levels also showed greater levels during DP with the highest at ZT20 compared with ZT0 (Fig. 9*B*). In line with the increased serum FGF23 levels during DP, expression of *Slc34a1* and *Slc34a3* coding for NaP_i-IIa and NaP_i-IIc, respectively, showed decreased expressions during DP (Fig. 9, *C* and *D*, and supplemental Fig. S1), suggesting the enhanced phosphate excretion in the urine during this period. Indeed, serum phosphate concentrations showed a decline during DP associated with enhanced phosphate excretion in the urine (Fig. 9, *E* and *F*). We also analyzed the expression profile of *Cyp27b1* and *Cyp24a1*, other target genes of FGF23 signaling in the kidney, and found that these genes exhibited circadian profiles (Fig. 10). The expression of *Cyp27b1*, which was down-regulated by FGF23 activation, was lower during the DP when FGF23 levels were greater, but the circadian profile of *Cyp24a1*, which was up-regulated by FGF23 activation, did not show any association with that of FGF23, suggesting that circadian profile of genes involved in vitamin D metabolism is mainly regulated by the circadian network independent of circadian FGF23 profiles.

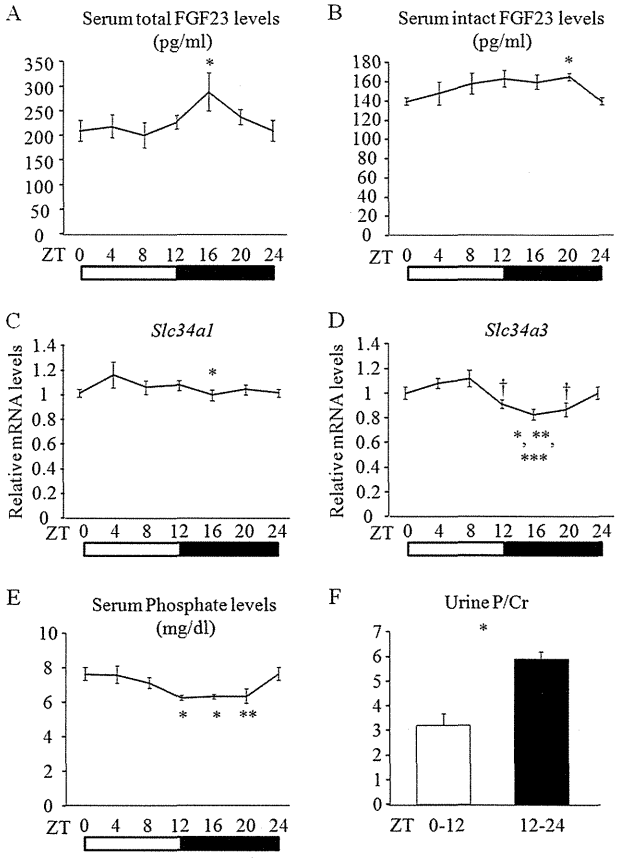

FIGURE 9. **Increase in skeletal *Fgf23* expression during the dark phase was associated with elevated circulating FGF23 levels and enhanced phosphate excretion in the urine.** WT mice were maintained under a light-dark regimen (12-h:12-h cycle) and fed *ad libitum*. Samples were collected every 4 h from ZT0. *A* and *B*, serum concentrations of total (C terminus) FGF23 (n = 6–7, *, $p < 0.05$ *versus* ZT0 and ZT8) (*A*) and intact (full-length) FGF23 (n = 6–7, *, $p < 0.05$ *versus* ZT0) (*B*) were measured. *C* and *D*, the expression of *slc34a1* (n = 6–7, *, $p < 0.05$ *versus* ZT4) (*C*) and *slc34a3* (n = 6–7, *, $p < 0.001$ *versus* ZT8; **, $p < 0.01$ *versus* ZT4; ***, $p < 0.05$ *versus* ZT0; †, $p < 0.05$ *versus* ZT4 and ZT8) (*D*) in the kidney was determined by real-time RT-PCR. *E*, serum concentration of phosphate was measured (n = 7, *, $p < 0.01$ *versus* ZT0; **, $p < 0.05$ *versus* ZT0). *F*, urine was collected either during the light phase (ZT0–12) or dark phase (ZT12–24), and phosphate and creatinine (*Cr*) levels in the urine were measured (n = 9, *, $p < 0.001$). The *white bar* and *black bar* represent the light phase and dark phase, respectively. Values are expressed as the mean ± S.E. (*error bars*).

DISCUSSION

In the present study, we demonstrated that skeletal *Fgf23* expression possessed a circadian expression profile. Importantly, the peak in skeletal *Fgf23* expression shifted when mice were maintained under LP-RF regimen, suggesting that timing of food intake is an important determinant for rhythmic expression profile of skeletal *Fgf23*. To investigate the mechanism responsible for generating the rhythmicity in skeletal *Fgf23* expression, we had a hypothesis that sympathetic activity may be the responsible factor linking food intake and skeletal

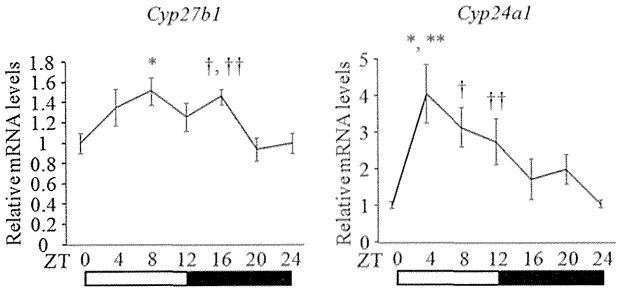

FIGURE 10. **Circadian expression profiles of genes involved in vitamin D metabolism in the kidney.** WT mice were maintained under a light-dark regimen (12-h:12-h cycle) and fed *ad libitum*. Samples were collected every 4 h from ZT0. The expression of *Cyp27b1* ($n = 8–10$, *, $p < 0.01$ *versus* ZT0 and ZT20; †, $p < 0.01$ *versus* ZT20; ††, $p < 0.05$ *versus* ZT0) and *Cyp24a1* ($n = 9–10$, *, $p < 0.001$ *versus* ZT0; **, $p < 0.01$ *versus* ZT16 and ZT20; †, $p < 0.01$ *versus* ZT0; ††, $p < 0.05$ *versus* ZT0) in the kidney was determined by real-time RT-PCR. The *white bar* and *black bar* represent the light phase and dark phase, respectively. Values are expressed as the mean ± S.E. (*error bars*).

Fgf23 expression based on the previous findings that sympathetic activation has been shown to be associated with food intake (28) and display a circadian profile with greater levels during the DP when food intake is active in mice (34). Indeed, we found that the administration of ISO caused an elevation in skeletal *Fgf23* expression in a circadian rhythm-dependent manner. Furthermore, the blockade of sympathetic activity by PRO in mice under LP-RF conditions altered the circadian *Fgf23* expression profile such that the peak expression of *Fgf23* was not observed. Importantly, LP-RF caused a phase shift in sympathetic activity with greater levels during the LF. These results imply that sympathetic activation driven by food intake is a positive regulator for skeletal *Fgf23* expression.

One of the important issues to be addressed is the effect of circadian regulation of skeletal *Fgf23* expression on systemic phosphate metabolism. To address this issue we performed series of analyses and found that circulating both total and biologically active (intact) FGF23 levels were greater during DP. In line with the increase in FGF23 levels during DP, the expression of *slc34a1* and *slc34a3*, known to be down-regulated by FGF23 activation in the kidney, was decreased during this period associated with enhanced phosphate excretion in the urine and decreased phosphate levels in the serum. Because food intake is increased at the beginning of DP in mice, these findings may suggest that the increase in skeletal *Fgf23* expression during DP has an important role in handling the phosphate influx from the diet. It is important to note that the amplitude of circadian profile of intact FGF23 levels is not as obvious as that of total FGF23 levels, suggesting the possibility of the existence of additional mechanism regulating circadian profile of intact FGF23 in the circulation. Because FGF23 protein is known to be cleaved between Arg-179 and Ser-180 (39), it is possible that the post-translational modification or processing of FGF23 protein may create the difference in amplitude between total and intact FGF23 circadian rhythms, although the mechanisms of how FGF23 is cleaved in the circulation are not well defined and still need to be determined. Thus, these lines of evidence may imply that the circadian clock network may function in a coordinated manner involving multiple organs to maintain systemic phosphate homeostasis.

The present findings demonstrate that the timing of food intake regulates the circadian profile of skeletal *Fgf23* expression, but it is still unclear as to whether circadian *Fgf23* expression is regulated by the influx of phosphate from the diet. Because inorganic phosphate has been shown to induce *Fgf23* expression in osteocyte-like IDG-SW3 cells (40), it is possible that the influx of phosphate from the diet may regulate circadian *Fgf23* expression; however, previous *in vivo* studies failed to demonstrate an acute effect of dietary phosphate on FGF23 induction (41, 42), making this concept unlikely to be operative. Despite the lack of an increase in FGF23 levels in response to an acute phosphate load, it has been well established that a chronic phosphate load causes elevations in FGF23 levels (43). Consistent with previous reports, we detected a significant increase in skeletal *Fgf23* expression in mice fed a high phosphate diet, but this increase was not associated with sympathetic activation because the concomitant administration of PRO did not affect *Fgf23* expression. These findings may indicate that the timing of food intake, and not the amount of ingested phosphate, is a predominant determinant for the circadian profiles of skeletal *Fgf23* expression.

The involvement of Cry1 in the regulation of G protein-coupled receptor signaling pathways has been demonstrated previously in a mouse model in which CRE activated luciferase activity in the liver (36). In these mice luciferase activity in the liver was markedly higher at ZT13 than at ZT1, which was associated with increased CREB phosphorylation, and was inhibited when Cry1 was overexpressed (36). The underlying mechanisms described in this study included the suppression of cAMP accumulation by binding of Cry1 to $G_s\alpha$ proteins (36). Based on these previous findings, we investigated whether a similar mechanism was operative in osteoblastic cells and found that overexpression of Cry1 suppressed ISO-induced CREB phosphorylation and trans-activation of the *Fgf23* promoter in osteoblastic UMR-106 cells, which indicated that Cry1 also suppressed ISO-induced *Fgf23* expression in osteoblastic cells. CREB has been shown to bind to the palindromic sequence (TGACGTCA) called CRE with strong affinity and regulate the transcription of target genes. In addition to this canonical CRE, CREB has also been shown to bind to CRE variants albeit with low affinity (44). The sequence of CRE detected in this study is one such variant that is known to mediate CREB signaling (44), and this may be one of the reasons why the induction of luciferase activity by ISO was not intense. Because *in vivo* analysis revealed a significant increase in *Fgf23* expression by the ISO treatment, other CRE motif(s) may be present in other regions and affect the *in vivo* expression of *Fgf23*.

The regulation of *Fgf23* expression in bone has also been implicated in the action of PTH. For example, circulating FGF23 levels were shown to be elevated under conditions in which PTH signaling was continuously active such as chronic kidney disease and Jansen metaphyseal chondrodysplasia caused by a mutation in the *PTH1R* gene, which suggests that PTH is a positive regulator for *Fgf23* expression (37, 45). However, the negative action of PTH on *Fgf23* expression has also been demonstrated in a mouse model in which PTH was intermittently administered (46). Thus, the effect of PTH on *Fgf23* expression is context-specific and controversial (37, 45–47).

Hence, the result showing that the induction of skeletal *Fgf23* by a single injection of PTH was observed in a circadian manner may provide a clue to solve this controversial issue of PTH action on *Fgf23* expression although further studies are needed to precisely determine PTH action on *Fgf23* regulation.

In conclusion, in the present study we have provided evidence that the time of food intake determined the circadian profile of skeletal *Fgf23* expression which involved a systemic activation of sympathetic tone and that sympathetic activation was peripherally regulated by Cry1 expression in the skeleton. Given the paucity of data as to the mechanisms regulating skeletal *Fgf23* expression, these lines of evidence may shed light on new regulatory networks of FGF23 which could be important for understanding the physiology of phosphate metabolism.

Acknowledgments—We thank Yasuhisa Ohata, Jin Nishino, Miwa Yamazaki, and Kanako Tachikawa (Osaka Medical Center and Research Institute for Maternal and Child Health) for critical discussions.

REFERENCES

1. Bergwitz, C., and Jüppner, H. (2011) Phosphate sensing. *Adv. Chronic Kidney Dis.* **18,** 132–144
2. Razzaque, M. S. (2012) The role of Klotho in energy metabolism. *Nat. Rev. Endocrinol.* **8,** 579–587
3. Hubbard, S. R., and Till, J. H. (2000) Protein-tyrosine kinase structure and function. *Annu. Rev. Biochem.* **69,** 373–398
4. Quarles, L. D. (2012) Skeletal secretion of FGF-23 regulates phosphate and vitamin D metabolism. *Nat. Rev. Endocrinol.* **8,** 276–286
5. Martin, A., David, V., and Quarles, L. D. (2012) Regulation and function of the FGF23/Klotho endocrine pathways. *Physiol. Rev.* **92,** 131–155
6. Shimada, T., Kakitani, M., Yamazaki, Y., Hasegawa, H., Takeuchi, Y., Fujita, T., Fukumoto, S., Tomizuka, K., and Yamashita, T. (2004) Targeted ablation of *Fgf23* demonstrates an essential physiological role of FGF23 in phosphate and vitamin D metabolism. *J. Clin. Invest.* **113,** 561–568
7. Urakawa, I., Yamazaki, Y., Shimada, T., Iijima, K., Hasegawa, H., Okawa, K., Fujita, T., Fukumoto, S., and Yamashita, T. (2006) Klotho converts canonical FGF receptor into a specific receptor for FGF23. *Nature* **444,** 770–774
8. Kuro-o, M., Matsumura, Y., Aizawa, H., Kawaguchi, H., Suga, T., Utsugi, T., Ohyama, Y., Kurabayashi, M., Kaname, T., Kume, E., Iwasaki, H., Iida, A., Shiraki-Iida, T., Nishikawa, S., Nagai, R., and Nabeshima, Y. I. (1997) Mutation of the mouse *klotho* gene leads to a syndrome resembling ageing. *Nature* **390,** 45–51
9. Kurosu, H., Ogawa, Y., Miyoshi, M., Yamamoto, M., Nandi, A., Rosenblatt, K. P., Baum, M. G., Schiavi, S., Hu, M. C., Moe, O. W., and Kuro-o, M. (2006) Regulation of fibroblast growth factor-23 signaling by Klotho. *J. Biol. Chem.* **281,** 6120–6123
10. ADHR Consortium. (2000) Autosomal dominant hypophosphataemic rickets is associated with mutations in FGF23. *Nat. Genet.* **26,** 345–348
11. Feng, J. Q., Ward, L. M., Liu, S., Lu, Y., Xie, Y., Yuan, B., Yu, X., Rauch, F., Davis, S. I., Zhang, S., Rios, H., Drezner, M. K., Quarles, L. D., Bonewald, L. F., and White, K. E. (2006) Loss of DMP1 causes rickets and osteomalacia and identifies a role for osteocytes in mineral metabolism. *Nat. Genet.* **38,** 1310–1315
12. Lorenz-Depiereux, B., Schnabel, D., Tiosano, D., Häusler, G., and Strom, T. M. (2010) Loss-of-function *ENPP1* mutations cause both generalized arterial calcification of infancy and autosomal-recessive hypophosphatemic rickets. *Am. J. Hum. Genet.* **86,** 267–272
13. Liu, S., Tang, W., Zhou, J., Stubbs, J. R., Luo, Q., Pi, M., and Quarles, L. D. (2006) Fibroblast growth factor 23 is a counter-regulatory phosphaturic hormone for vitamin D. *J. Am. Soc. Nephrol.* **17,** 1305–1315
14. Shimada, T., Yamazaki, Y., Takahashi, M., Hasegawa, H., Urakawa, I., Oshima, T., Ono, K., Kakitani, M., Tomizuka, K., Fujita, T., Fukumoto, S., and Yamashita, T. (2005) Vitamin D receptor-independent FGF23 actions in regulating phosphate and vitamin D metabolism. *Am. J. Physiol. Renal Physiol.* **289,** F1088–F1095
15. Kolek, O. I., Hines, E. R., Jones, M. D., LeSueur, L. K., Lipko, M. A., Kiela, P. R., Collins, J. F., Haussler, M. R., and Ghishan, F. K. (2005) 1α,25-Dihydroxyvitamin D3 up-regulates FGF23 gene expression in bone: the final link in a renal-gastrointestinal-skeletal axis that controls phosphate transport. *Am. J. Physiol. Gastrointest. Liver Physiol.* **289,** G1036–G1042
16. Nelson, W. (1964) Aspects of circadian periodic changes in phosphorus metabolism in mice. *Am. J. Physiol.* **206,** 589–598
17. Carpenter, T. O., Insogna, K. L., Zhang, J. H., Ellis, B., Nieman, S., Simpson, C., Olear, E., and Gundberg, C. M. (2010) Circulating levels of soluble Klotho and FGF23 in X-linked hypophosphatemia: circadian variance, effects of treatment, and relationship to parathyroid status. *J. Clin. Endocrinol. Metab.* **95,** E352–E357
18. Smith, E. R., Cai, M. M., McMahon, L. P., and Holt, S. G. (2012) Biological variability of plasma intact and C-terminal FGF23 measurements. *J. Clin. Endocrinol. Metab.* **97,** 3357–3365
19. Vollmers, C., Gill, S., DiTacchio, L., Pulivarthy, S. R., Le, H. D., and Panda, S. (2009) Time of feeding and the intrinsic circadian clock drive rhythms in hepatic gene expression. *Proc. Natl. Acad. Sci. U.S.A.* **106,** 21453–21458
20. Green, C. B., Takahashi, J. S., and Bass, J. (2008) The meter of metabolism. *Cell* **134,** 728–742
21. Bass, J., and Takahashi, J. S. (2010) Circadian integration of metabolism and energetics. *Science* **330,** 1349–1354
22. Liu, C., Li, S., Liu, T., Borjigin, J., and Lin, J. D. (2007) Transcriptional coactivator PGC-1α integrates the mammalian clock and energy metabolism. *Nature* **447,** 477–481
23. Damiola, F., Le Minh, N., Preitner, N., Kornmann, B., Fleury-Olela, F., and Schibler, U. (2000) Restricted feeding uncouples circadian oscillators in peripheral tissues from the central pacemaker in the suprachiasmatic nucleus. *Genes Dev.* **14,** 2950–2961
24. Zhang, L., Abraham, D., Lin, S. T., Oster, H., Eichele, G., Fu, Y. H., and Ptáček, L. J. (2012) PKCγ participates in food entrainment by regulating BMAL1. *Proc. Natl. Acad. Sci. U.S.A.* **109,** 20679–20684
25. Fagius, J., and Berne, C. (1994) Increase in muscle nerve sympathetic activity in humans after food intake. *Clin. Sci.* **86,** 159–167
26. Sakaguchi, T., Arase, K., Fisler, J. S., and Bray, G. A. (1988) Effect of starvation and food intake on sympathetic activity. *Am. J. Physiol.* **255,** R284–R288
27. Troisi, R. J., Weiss, S. T., Parker, D. R., Sparrow, D., Young, J. B., and Landsberg, L. (1991) Relation of obesity and diet to sympathetic nervous system activity. *Hypertension* **17,** 669–677
28. Tseng, Y. H., Cypess, A. M., and Kahn, C. R. (2010) Cellular bioenergetics as a target for obesity therapy. *Nat. Rev. Drug Discov.* **9,** 465–482
29. Ralph, M. R., Foster, R. G., Davis, F. C., and Menaker, M. (1990) Transplanted suprachiasmatic nucleus determines circadian period. *Science* **247,** 975–978
30. Kornmann, B., Schaad, O., Bujard, H., Takahashi, J. S., and Schibler, U. (2007) System-driven and oscillator-dependent circadian transcription in mice with a conditionally active liver clock. *PLoS Biol.* **5,** e34
31. Shimba, S., Ogawa, T., Hitosugi, S., Ichihashi, Y., Nakadaira, Y., Kobayashi, M., Tezuka, M., Kosuge, Y., Ishige, K., Ito, Y., Komiyama, K., Okamatsu-Ogura, Y., Kimura, K., and Saito, M. (2011) Deficient of a clock gene, brain and muscle Arnt-like protein-1 (BMAL1), induces dyslipidemia and ectopic fat formation. *PLoS One* **6,** e25231
32. Kondo, H., Nifuji, A., Takeda, S., Ezura, Y., Rittling, S. R., Denhardt, D. T., Nakashima, K., Karsenty, G., and Noda, M. (2005) Unloading induces osteoblastic cell suppression and osteoclastic cell activation to lead to bone loss via sympathetic nervous system. *J. Biol. Chem.* **280,** 30192–30200
33. Takeda, S., Elefteriou, F., Levasseur, R., Liu, X., Zhao, L., Parker, K. L., Armstrong, D., Ducy, P., and Karsenty, G. (2002) Leptin regulates bone formation via the sympathetic nervous system. *Cell* **111,** 305–317
34. Fu, L., Patel, M. S., Bradley, A., Wagner, E. F., and Karsenty, G. (2005) The molecular clock mediates leptin-regulated bone formation. *Cell* **122,** 803–815
35. Elefteriou, F., Ahn, J. D., Takeda, S., Starbuck, M., Yang, X., Liu, X., Kondo,

H., Richards, W. G., Bannon, T. W., Noda, M., Clement, K., Vaisse, C., and Karsenty, G. (2005) Leptin regulation of bone resorption by the sympathetic nervous system and CART. *Nature* **434,** 514–520
36. Zhang, E. E., Liu, Y., Dentin, R., Pongsawakul, P. Y., Liu, A. C., Hirota, T., Nusinow, D. A., Sun, X., Landais, S., Kodama, Y., Brenner, D. A., Montminy, M., and Kay, S. A. (2010) Cryptochrome mediates circadian regulation of cAMP signaling and hepatic gluconeogenesis. *Nat. Med.* **16,** 1152–1156
37. Lavi-Moshayoff, V., Wasserman, G., Meir, T., Silver, J., and Naveh-Many, T. (2010) PTH increases *FGF23* gene expression and mediates the high-*FGF23* levels of experimental kidney failure: a bone parathyroid feedback loop. *Am. J. Physiol. Renal Physiol.* **299,** F882–F889
38. Keller, H., and Kneissel, M. (2005) *SOST* is a target gene for PTH in bone. *Bone* **37,** 148–158
39. Benet-Pagès, A., Lorenz-Depiereux, B., Zischka, H., White, K. E., Econs, M. J., and Strom, T. M. (2004) FGF23 is processed by proprotein convertases but not by PHEX. *Bone* **35,** 455–462
40. Ito, N., Findlay, D. M., Anderson, P. H., Bonewald, L. F., and Atkins, G. J. (2013) Extracellular phosphate modulates the effect of 1α,25-dihydroxy vitamin D3 (1,25D) on osteocyte like cells. *J. Steroid Biochem. Mol. Biol.* **136,** 183–186
41. Larsson, T., Nisbeth, U., Ljunggren, O., Jüppner, H., and Jonsson, K. B. (2003) Circulating concentration of FGF-23 increases as renal function declines in patients with chronic kidney disease, but does not change in response to variation in phosphate intake in healthy volunteers. *Kidney Int.* **64,** 2272–2279
42. Nishida, Y., Taketani, Y., Yamanaka-Okumura, H., Imamura, F., Taniguchi, A., Sato, T., Shuto, E., Nashiki, K., Arai, H., Yamamoto, H., and Takeda, E. (2006) Acute effect of oral phosphate loading on serum fibroblast growth factor 23 levels in healthy men. *Kidney Int.* **70,** 2141–2147
43. Perwad, F., Azam, N., Zhang, M. Y., Yamashita, T., Tenenhouse, H. S., and Portale, A. A. (2005) Dietary and serum phosphorus regulate fibroblast growth factor 23 expression and 1,25-dihydroxyvitamin D metabolism in mice. *Endocrinology* **146,** 5358–5364
44. Smith, B., Fang, H., Pan, Y., Walker, P. R., Famili, A. F., and Sikorska, M. (2007) Evolution of motif variants and positional bias of the cyclic-AMP response element. *BMC Evol. Biol.* **7,** S15
45. Brown, W. W., Jüppner, H., Langman, C. B., Price, H., Farrow, E. G., White, K. E., and McCormick, K. L. (2009) Hypophosphatemia with elevations in serum fibroblast growth factor 23 in a child with Jansen's metaphyseal chondrodysplasia. *J. Clin. Endocrinol. Metab.* **94,** 17–20
46. Samadfam, R., Richard, C., Nguyen-Yamamoto, L., Bolivar, I., and Goltzman, D. (2009) Bone formation regulates circulating concentrations of fibroblast growth factor 23. *Endocrinology* **150,** 4835–4845
47. Saji, F., Shigematsu, T., Sakaguchi, T., Ohya, M., Orita, H., Maeda, Y., Ooura, M., Mima, T., and Negi, S. (2010) Fibroblast growth factor 23 production in bone is directly regulated by 1α,25-dihydroxyvitamin D, but not PTH. *Am. J. Physiol. Renal Physiol.* **299,** F1212–F1217

Bone 67 (2014) 56–62

Contents lists available at ScienceDirect

Bone

journal homepage: www.elsevier.com/locate/bone

Case Report

Hypophosphatemic osteomalacia and bone sclerosis caused by a novel homozygous mutation of the FAM20C gene in an elderly man with a mild variant of Raine syndrome

Shinji Takeyari [a], Takehisa Yamamoto [a,*], Yuka Kinoshita [b], Seiji Fukumoto [b], Francis H. Glorieux [c], Toshimi Michigami [d], Kosei Hasegawa [e], Taichi Kitaoka [f], Takuo Kubota [f], Yasuo Imanishi [g], Tsunesuke Shimotsuji [a], Keiichi Ozono [f]

[a] Department of Pediatrics, Minoh City Hospital, Osaka 562-8562, Japan
[b] Division of Nephrology and Endocrinology, Department of Medicine, The University of Tokyo Hospital, Tokyo 113-8655, Japan
[c] Genetics Unit, Shriners Hospitals for Children, Montreal H3G 1A6, Canada
[d] Department of Bone and Mineral Research, Osaka Medical Center and Research Institute for Maternal and Child Health, Osaka 594-1011, Japan
[e] Department of Pediatrics, Okayama University Hospital, Okayama 700-8558, Japan
[f] Department of Pediatrics, Osaka University Graduate School of Medicine, Osaka 565-0871, Japan
[g] Department of Metabolism, Endocrinology and Molecular Medicine, Osaka City University Graduate School of Medicine, Osaka 545-8585, Japan

ARTICLE INFO

Article history:
Received 2 February 2014
Revised 19 June 2014
Accepted 20 June 2014
Available online 27 June 2014

Edited by: Bente Langdahl

Keywords:
FAM20C
Hypophosphatemic rickets
FGF23
Loss of teeth
OPLL
Cortical hyperostosis

ABSTRACT

Background: Hypophosphatemia and increased serum fibroblast growth factor 23 (FGF23) levels have been reported in young brothers with compound heterozygous mutations for the FAM20C gene; however, rickets was not observed in these cases. We report an adult case of Raine syndrome accompanying hypophosphatemic osteomalacia with a homozygous *FAM20C* mutation (R408W) associated with increased periosteal bone formation in the long bones and an increase in bone mineral density in the femoral neck.
Case: The patient, a 61-year-old man, was born from a cousin-to-cousin marriage. A short stature and severe dental demineralization were reported at an elementary school age. Hypophosphatemia was noted inadvertently at 27 years old, at which time he started to take an active vitamin D metabolite (alphacalcidol) and phosphate. He also manifested ossification of the posterior longitudinal ligament. On bone biopsy performed at the age of 41 years, we found severe osteomalacia surrounding osteocytes, which appeared to be an advanced form of periosteocytic hypomineralized lesions compared to those reported in patients with X-linked hypophosphatemic rickets. Laboratory data at 61 years of age revealed markedly increased serum intact-FGF23 levels, which were likely to be the cause of hypophosphatemia and the decreased level of $1,25(OH)_2D$. We recently identified a homozygous *FAM20C* mutation, which was R408W, in this patient. When expressed in HEK293 cells, the R408W mutant protein exhibited impaired kinase activity and secretion.
Discussion: Our findings suggest that certain homozygous *FAM20C* mutations can cause FGF23-related hypophosphatemic osteomalacia and indicate the multiple roles of FAM20C in bone.

Introduction

In 1989, Raine syndrome was first reported as a lethal disease with generalized osteosclerotic bone dysplasia inherited in an autosomal recessive fashion [1]. It is characterized by increased periosteal bone formation, which differs from osteopetrosis [2]. In 2007, *FAM20C* was identified as the gene responsible for a lethal type of Raine syndrome [3], and about 24 patients were previously reported [4,5]. However, *FAM20C* is also associated with a non-lethal type of Raine syndrome with generalized osteosclerosis. In 2009, two patients with this type of Raine syndrome were reported and one patient showed hypophosphatemia [6]. In 2013, Rafaelsen et al. reported that patients with compound heterozygous mutations in this gene had hypophosphatemia due to increased serum fibroblast growth factor 23 (FGF23) levels [7]. In addition, homozygous inactivation of *FAM20C* leads to hypophosphatemic rickets in mice [8]. These results indicate that the FAM20C gene is responsible for the distinct type of autosomal recessive hypophosphatemia with abnormal bone metabolism.

Concerning the function of *FAM20C* products, *FAM20C* encodes a Golgi kinase that phosphorylates proteins [9] including small integrin-binding ligand N-linked glycoproteins (SIBLINGs) [10], some of which

* Corresponding author at: Department of Pediatrics, Minoh City Hospital, 5-7-1 Kayano, Minoh City, Osaka 562-8562, Japan. Fax: +81 727 28 8495.
E-mail address: t.yamamoto@minoh-hp.jp (T. Yamamoto).

http://dx.doi.org/10.1016/j.bone.2014.06.026
8756-3282/

are known to be inhibitors of mineralization through binding to hydroxyapatite [11]. Thus, a physiological function of FAM20C may be to inhibit mineralization. From a clinical point of view, mutations of the FAM20C gene in patients with Raine syndrome are considered to be inactivating ones because the disease is transmitted in an autosomal recessive fashion. Therefore, inactivation of the FAM20C gene may be associated with osteosclerosis in patients with Raine syndrome due to the promotion of mineralization. However, this hypothesis cannot explain the cause of hypophosphatemia due to increased serum FGF23 levels [7]. The increased production of FGF23 by bone tissues as well as hypophosphatemic rickets has also been reported in the *FAM20C* knock-out (KO) mouse model [8]. These observations suggest that FAM20C gene abnormalities may cause both hypophosphatemic disease and osteosclerosis at the same time.

In addition, Raine syndrome is associated with features that are different from those found in FGF23-related hypophosphatemic rickets such as X-linked hypophosphatemic rickets (XLH), autosomal dominant hypophosphatemic rickets (ADHR), and autosomal recessive hypophosphatemic rickets (ARHR) 1 and 2 [12]. These features are intracerebral calcification and a higher incidence of dental anomalies. Since severe cases of Raine syndrome are lethal, it is unlikely that mutant proteins have no enzymatic activity in adult patients. However, the residual activity of mutated FAM20C found in patients with FGF23-related hypophosphatemia has not been shown in function assays [7].

Here, we report the case of an elderly man with a non-lethal variant of Raine syndrome caused by a homozygous R408W mutation in the FAM20C gene associated with hypophosphatemic osteomalacia, increased periosteal bone formation and femoral neck bone mineral density, early loss of teeth, and intracerebral calcification. The R408W mutant exhibited residual kinase activity that phosphorylated osteopontin.

Materials and methods

Laboratory data

General laboratory data were obtained at Minoh City Hospital, Osaka, Japan. Serum 1,25-dihydroxyvitamin D (1,25$(OH)_2$D) and 25-hydroxyvitamin D (25OHD) levels were measured with a radioreceptor assay and competitive protein binding assay, respectively. Serum intact and high sensitive parathyroid hormone levels were measured with an electrochemiluminescent immunoassay and a radioimmunoassay, respectively. Serum intact FGF23 (iFGF23) levels were measured with the FGF-23 ELISA Kit (Kainos Inc., Tokyo, Japan).

The maximal tubular reabsorption of phosphate per glomerular filtration rate (TmP/GFR) was calculated with Bijvoet's nomogram [13]. The bone mineral density was measured with a dual-energy X-ray absorptiometry (DXA) scanner (Hologic Inc., Bedford, MA, USA).

Mutational analysis

Genomic DNA was extracted from peripheral blood using the QIAamp DNA Blood Mini Kit (QIAGEN, Tokyo, Japan). All coding exons and exon–intron junctions of the PHEX, DMP1, ENPP1, FGF23, and FAM20C genes were amplified by PCR. PCR products were then gel-purified using NucleoSpin® Gel and PCR Clean-up (Macherey-Nagel, Duren, Germany) and directly sequenced by dye-deoxy termination cycle sequencing using the same primers. Primer sequences can be obtained upon request.

Construction of expression vectors

Human FAM20C cDNA was amplified by RT-PCR from peripheral blood leukocytes and cloned into pcDNA 3.1/*myc*-His A (Invitrogen) with the In-Fusion HD Cloning Kit (Clontech). Human OPN cDNA was amplified by PCR with pDest490-OPN-a (Addgene plasmid 17590) as a template and similarly cloned into pcDNA 3.1/*myc*-His A.

Site-specific mutagenesis was performed using the PrimeSTAR Mutagenesis Basal Kit (TAKARA BIO), PrimeSTAR HS DNA polymerase with GC Buffer (TAKARA BIO), or Tks Gflex DNA polymerase (TAKARA BIO). Primer sequences are available upon request.

Functional analysis of FAM20C

HEK293 cells were grown in 6-well dishes to 70–80% confluency and transfected with 2 μg of pcDNA 3.1/*myc*-His A-FAM20C (or mutants) with 5 μL of FuGENE-HD (Roche) as recommended by the manufacturer. Cells were transfected with 0.4 μg of pcDNA 3.1/*myc*-His A-FAM20C (or mutants) and 1.6 μg of pcDNA 3.1/*myc*-His A-OPN for co-transfection analysis. The medium was replaced with 1 mL of Opti-MEM Reduced Serum Medium 24 h after transfection. Conditioned medium was removed 48 to 72 h after transfection and centrifuged at 1000 ×g for 5 min to remove cell debris. Cells were washed twice with PBS and lysed with 500 μL of Opti-MEM Reduced Serum Medium, 55 μL of FastBreak Cell Lysis Reagent (Promega), 5 μL of Protease Inhibitor, and 0.5 μL of DNaseI for 20 min. The cell lysate was centrifuged at 13,000 ×g for 10 min and the supernatant was collected. The MagneHis Protein Purification System (Promega) was used to purify polyhistidine-tagged FAM20C and osteopontin, as recommended by the manufacturer. A 10-μL aliquot from 100 μL of the elutant was separated by SDS-PAGE and transferred to a PVDF membrane, which was blocked in ImmunoBlock (DS Pharma Biomedical) and probed with an anti-c-Myc antibody (Santa Cruz Biotechnology) overnight at 4 °C. The membrane was then incubated with an anti-mouse IgG antibody with horseradish peroxidase (GE Healthcare) for 1 h at room temperature. The ECL Select Western Blotting Detection Reagent (GE Healthcare) was used for chemiluminescent detection.

Bone histology

The patient underwent lumbar fenestration surgery at the age of 41 years old due to intermittent claudication and numbness of both legs, during which time iliac bone biopsy was performed. Bone specimens were fixed in neutral formaldehyde, dehydrated in ethanol, and embedded in methylmethacrylate, followed by the preparation of undecalcified sections. Sections were stained with Villanueva bone stain in Japan followed by Goldner staining at Shriners Hospitals for Children in Montreal, Canada.

Ethics

The study protocol was approved by the Review Board of the Minoh City Hospital Clinical Ethics Committee. We obtained informed consent from the patient using written documents.

Case report

The patient is a 61-year-old Japanese man born from a cousin-to-cousin marriage. His weight and height at 58 years old were 61 kg (−0.67 SD) and 153 cm (−2.8 SD), respectively. His sister and brother did not have a short stature or symptoms of metabolic bone diseases. Although he had mild bowlegs in childhood, his short stature was initially reported at an elementary school age. He had lost all his teeth by the age of 17 years as they had been gradually worn down (Fig. 1). He had no history of abscessed teeth, and the lost teeth were replaced with dentures. He was incidentally diagnosed with hypophosphatemia associated with elevated urinary loss of phosphate at 27 years old; however, no tumors were found on computerized tomography (CT) scan and magnetic resonance imaging, which suggested that he did not have tumor-induced osteomalacia. He was treated with an active vitamin D metabolite (alphacalcidol) and phosphate. Ossification of the posterior

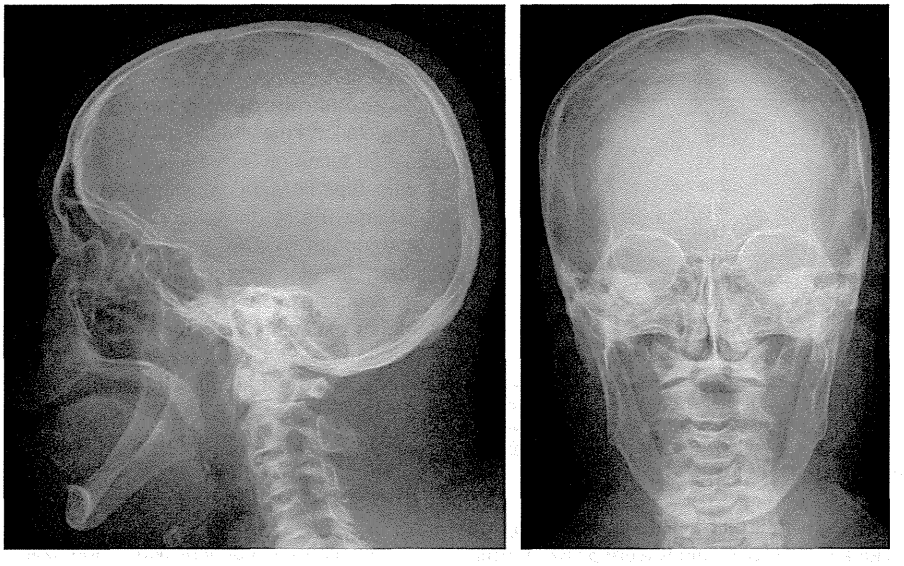

Fig. 1. Skull radiographs at the age of 61 years. Note the absence of teeth.

longitudinal ligament was revealed at the age of 35 years (Fig. 2). When the patient was 37 years old, we performed the Ellsworth–Howard test after 2 weeks of treatment discontinuation, and found normal responses of urinary phosphate and cyclic AMP excretions to exogenous parathyroid hormone (PTH).

His serum high sensitive parathyroid hormone level was slightly increased to 340 pg/mL (normal control: 90–270) at the age of 37 years. We stopped treatment with phosphate but continued active vitamin D administration at the age of 41 years because of a slightly deteriorated renal function, which was possibly derived from nephrocalcinosis because of the phosphate therapy. Bone biopsy specimens revealed large areas of osteomalacia surrounding osteocytes (Fig. 3), which appeared to be advanced forms of periosteocytic hypomineralized lesions compared to those reported in patients with X-linked hypophosphatemic rickets [14].

The most recent laboratory test following the cessation of therapy for 10 days when the patient was 61 years old revealed that his serum $1,25(OH)_2D$ level was low (12 pg/mL; normal range: 20–60) in spite of a decrease in his serum phosphate concentration (1.9 mg/dL; normal

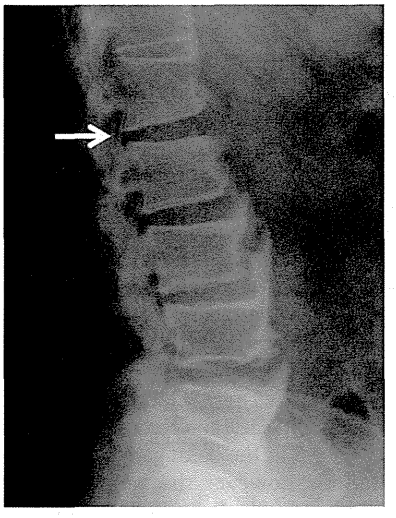

Fig. 2. A lumbar spine radiograph at the age of 50 years. Note anterior osteophytes with a coarse trabecular pattern from L3 to L5 regions. The arrow denotes ossification of the posterior longitudinal ligament.

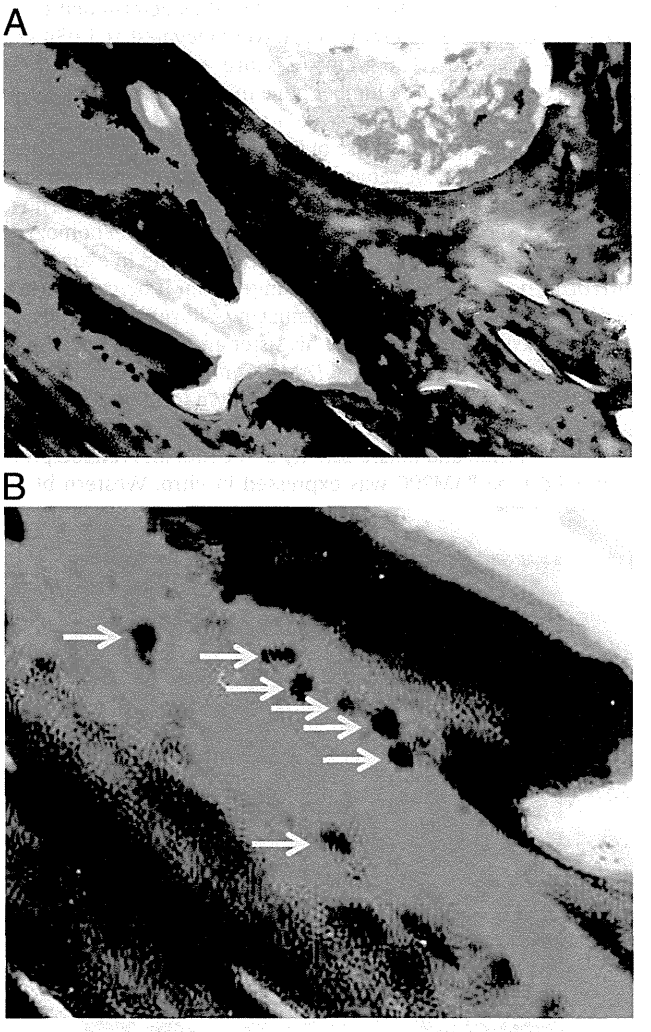

Fig. 3. (A) Iliac crest biopsy specimen was stained by Villanueva bone and Goldner's methods. Large areas of osteomalacia surrounding osteocytes were observed, being much more severe compared to hypomineralized periosteocytic lesions, halos of unmineralized bone surrounding osteocyte lacunae, reported in XLH patients. (B) A higher magnification of Fig. 3A. The arrows indicate osteocytes.

Table 1
Laboratory data at 61 years old (before and after stopping medication).

	Before	After	Reference range
Serum Ca (mg/dL)	10.3	9.2	8.7–11.0
Serum P (mg/dL)	2.1	1.9	2.7–4.4
Serum Cr (mg/dL)	1.40	1.31	0.6–1.1
ALP (IU/L)	347	288	104–338
Intact-PTH (pg/mL)	32	60	10–65
$1,25(OH)_2D$ (pg/mL)	52	12	20–60
25OHD (ng/mL)	27.1	ND	
Intact FGF23 (pg/mL)	386	309	10–50
Urine P (mg/dL)	70.3	32.0	0–80
Urine Cr (mg/dL)	145	52	
%TRP (%)	67.7	57.6	>80
TmP/GFR (mg/dL)	1.5	1.1	2.8–4.2

ND, not done; Ca, calcium; P, phosphorus; Cr, creatinine; ALP, alkaline phosphatase; PTH, parathyroid hormone; $1,25(OH)_2D$, 1,25-dihydroxyvitamin D; 25OHD, 25-hydroxyvitamin D; %TRP, percentage of tubular reabsorption of phosphate; and TmP/GFR, the maximal tubular reabsorption of phosphate per glomerular filtration rate.

range: 2.7–4.4) (Table 1). The serum intact-PTH level was 60 pg/mL (normal range: 10–65). %TRP and TmP/GFR values were 57.6% (normal range >80) and 1.1 mg/dL (normal range: 2.8–4.2), respectively. His serum iFGF23 level was elevated to 309 pg/mL (normal range: 10–50). We identified intracerebral calcification in the basal ganglia by CT (Fig. 4). Bone radiographs revealed increased periosteal bone formation in the humerus (Fig. 5). Bone mineral densities determined by DXA analysis in the bilateral femoral neck were elevated at 1.034 g/cm^2 (Z-score +2.5) and 1.156 g/cm^2 (Z-score +3.6) on the right and left sides, respectively. The lumber bone mineral density (L2–L4) was also elevated at 2.007 g/cm^2 (Z-score +6.3).

In order to identify the cause of FGF23-related hypophosphatemic disease in this patient, we sequenced all coding exons and exon–intron junctions in PHEX, DMP1, ENPP1, and FGF23 genes. However, no mutation was observed in these genes. In contrast, a novel homozygous missense mutation, c.1222C>T, R408W, was found in exon 6 of the FAM20C gene (Fig. 6). This base change has not been reported in the database (http://www.ncbi.nlm.nih.gov/SNP/snp_ref.cgi?locusId=56975). We could not investigate his sister and brother because they did not agree to genetic testing. *FAM20C* mutations associated with hypophosphatemia in the literature are shown in Table 2, confirming that R408W mutation has not previously been reported. We then analyzed the secretion and kinase activity of the mutant FAM20C protein. When wild-type FAM20C was expressed in vitro, Western blotting revealed more FAM20C protein in the conditioned medium than in the cell lysate (Fig. 7A).

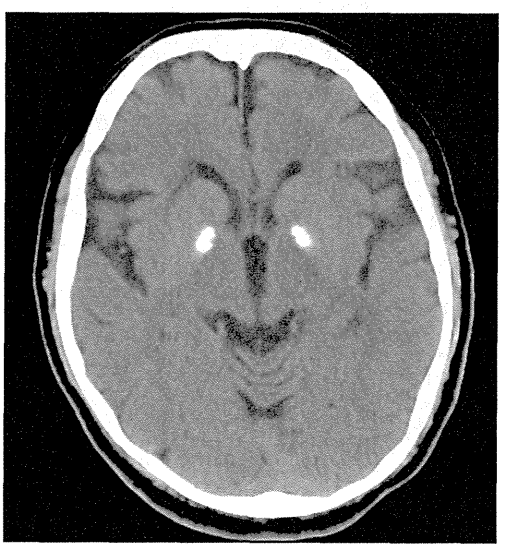

Fig. 4. Cranial computerized tomography at the age of 61 years. Note intra-cerebral calcification in the region of the basal ganglia.

In contrast, most R408W mutant protein was observed in the cell lysate, indicating that secretion of the mutant protein was impaired (Fig. 7A). A kinase-dead mutant (D478A) also exhibited partially impaired secretion (Fig. 7A), consistent with a previous report [9]. Since wild-type FAM20C was shown to increase the molecular weight of osteopontin by phosphorylation [9], the kinase activity of wild-type and mutant FAM20C proteins was examined by analyzing changes in the molecular weight of osteopontin. When wild-type FAM20C and osteopontin were co-expressed, phosphorylated osteopontin had a higher molecular weight than that of unphosphorylated osteopontin without FAM20C expression (Fig. 7B). The kinase-dead D478A mutant FAM20C did not alter the molecular weight of osteopontin, whereas the R408W mutant FAM20C slightly increased it, which indicated the impaired but residual kinase activity of this mutant protein (Fig. 7B).

Discussion

We reported a patient with a homozygous mutation in the FAM20C gene that was R408W. He had FGF23-related hypophosphatemic osteomalacia complicated by cortical hyperostosis and increased bone mineral density in the femoral neck and lumbar vertebrae, suggesting that the FAM20C gene has the dual effect of increasing bone formation and causing osteomalacia in humans.

FGF23-related hypophosphatemic rickets with a genetic background consists of XLH, ADHR, and two forms of ARHR (ARHR1 and ARHR2). The genes responsible for this type of rickets were identified as *PHEX*, *FGF23*, *DMP1*, and *ENPP1*, respectively [12]. The FAM20C gene was recently shown to be the gene responsible for autosomal recessive hypophosphatemia, although it was originally identified as the causal gene of Raine syndrome [3,6,7]. Since the loss-of-function mutations in *FAM20C* seem to impair the phosphorylation of SIBLING proteins, some of which are inhibitors of mineralization, and are expected to destroy the inhibitory function, osteomalacia was an unexpected observation. Thus, our patient suggested the possibility that hypophosphatemia due to the elevated serum levels of FGF23 partly overcomes the role of FAM20C in bone leading to osteomalacia. Thus, the present case provides additional evidence to show that the FAM20C gene may be responsible for ARHR in addition to DMP1 and ENPP1 gene, although we had no evidence that the patient suffered from rickets in childhood. Dental abnormalities have been reported in patients with ARHR1 [15]; however, the premature loss of teeth is rare [16]. In contrast, FAM20C was reported to be essential for the formation of murine teeth [17], and the premature loss of teeth was reported in patients with compound heterozygous mutations in *FAM20C* [7]. Our patient did not have a remarkable history of abscessed teeth. Moreover, his teeth were worn down, showing a gradually decreased volume. These findings are compatible with a recent report on the presence of amelogenesis imperfecta in *FAM20C* null mice [18]. Thus, the premature loss of teeth may be an index suggesting the presence of a *FAM20C* mutation in patients with sporadic non-lethal Raine syndrome with hypophosphatemia. In addition, hyperostosis of the cortical bones appears to be characteristic of these patients because no hyperostosis was reported in cortical bone in patients with ARHR1 or XLH. A recent study using peripheral quantitative computed tomography revealed a reduced bone mineral density in the forearms of XLH patients [19]. Thus, the clinical key to diagnosing hypophosphatemic rickets caused by mutations in *FAM20C* is the premature loss of teeth and coexistence of osteomalacia and cortical hyperostosis. The presence of cerebral calcification in the basal ganglia suggests the possibility of *FAM20C* mutations; however, the same findings have also been reported in healthy individuals [20] and patients with several diseases such as hypoparathyroidism and Fahr disease [21].

The mechanism by which osteomalacia coexists with cortical hyperostosis combined with an increased bone mineral density in the femoral